

# Stellar Models and Yields of Asymptotic Giant Branch Stars

Amanda Karakas<sup>A,C</sup> and John C. Lattanzio<sup>B</sup>

<sup>A</sup> Research School of Astronomy & Astrophysics, Mount Stromlo Observatory, Cotter Road Weston Creek, ACT 2611, Australia

<sup>B</sup> Centre for Stellar and Planetary Astrophysics, Monash University, PO Box 28M, Clayton VIC 3800, Australia

<sup>C</sup> Email: akarakas@mso.anu.edu.au

**Abstract:** We present stellar yields calculated from detailed models of low and intermediate-mass asymptotic giant branch (AGB) stars. We evolve models with a range of mass from 1 to  $6M_{\odot}$ , and initial metallicities from solar to  $1/200^{\text{th}}$  of the solar metallicity. Each model was evolved from the zero age main sequence to near the end of the thermally-pulsing AGB (TP-AGB) phase, and through all intermediate phases including the core He-flash for stars initially less massive than  $2.5M_{\odot}$ . For each mass and metallicity, we provide tables containing structural details of the stellar models during the TP-AGB phase, and tables of the stellar yields for 74 species from hydrogen through to sulphur, and for a small number of iron-group nuclei. All tables are available for download. Our results have many applications including use in population synthesis studies and the chemical evolution of galaxies and stellar systems, and for comparison to the composition of AGB and post-AGB stars and planetary nebulae.

**Keywords:** stars: AGB and post-AGB — abundances — ISM: abundances — planetary nebulae: general

## 1 Introduction

Stars with initial masses in the range  $\sim 0.8$  to  $8M_{\odot}$ , depending on the initial metallicity  $Z$ , will pass through the thermally-pulsing asymptotic giant branch (TP-AGB) phase before ending their lives as white dwarfs. The structure and evolution of low and intermediate mass stars prior to and during the AGB has been previously discussed in some detail (see Busso et al. 1999; Herwig 2005, and references therein). An AGB star is characterized by two nuclear burning shells, one burning helium (He) above a degenerate carbon-oxygen core and another burning hydrogen (H), below a deep convective envelope. In-between lies the intershell region composed mostly of  ${}^4\text{He}$ . The helium-burning shell is thermally unstable and flashes or pulses every  $10^4$  years or so. After the occurrence of a thermal pulse (TP), mixing episodes may occur that bring the products of nuclear burning from deep inside the star to the stellar surface. These mixing events, or third dredge-up (TDU) episodes, bring the products of partial He-burning (mostly  ${}^4\text{He}$  and  ${}^{12}\text{C}$ ) into the envelope. The TDU is the mechanism for turning (single) stars into carbon stars, where the C/O ratio exceeds unity in the surface layers. Following dredge-up the H-shell is re-ignited and the star enters a phase of quiescent H-burning known as the interpulse phase. The TP-AGB is defined as the phase from the first TP to the time when the star ejects its outer envelope, terminating the AGB phase.

In the most massive AGB models ( $M \gtrsim 4M_{\odot}$ , depending on the metallicity) hot bottom burning (HBB) can occur when the base of the convective envelope dips into the top of the H-shell resulting in a thin layer hot enough to sustain proton-capture nucleosynthesis. The convective turn-over time in the envelope is  $\sim 1$  year that ensures that the whole envelope is exposed to the hot region a few thousand times per interpulse period. There is observational evidence that HBB occurs in massive AGB stars (Wood et al. 1983; Smith & Lambert 1989; McSaveney et al. 2007) in the Large and Small Magellanic Clouds (LMC and SMC). HBB converts  ${}^{12}\text{C}$  into  ${}^{14}\text{N}$  and if the TDU is operating, HBB will prevent the atmosphere from becoming carbon rich (Boothroyd, Sackmann, & Ahern 1993). The copious amounts of  ${}^{14}\text{N}$  produced in this case will be primary<sup>1</sup> owing to the primary  ${}^{12}\text{C}$  being dredged from the He-shell. Frost et al. (1998) found intermediate-mass AGB evolution to be sensitive to the initial composition and the mass-loss law used in the calculation, with models becoming C-rich near the tip of the AGB if TDU continues after HBB has been shut off. The occurrence and duration of HBB depends upon the initial metallicity, mass loss and convection (Ventura & D’Antona 2005a) where the minimum mass for HBB is pushed to lower mass in lower metallicity models (Frost et al. 1998).

Owing to fact that calculating a TP-AGB model is a computationally intensive task, synthetic AGB models, which use fitting formulae to model the evolution quickly, have proved to be a successful approach to population synthesis studies that require large stellar populations. Historically this approach was validated by the fact that the stellar luminosity on the AGB is nearly a linear function of the H-exhausted core mass (e.g. Paczynski 1975; Renzini & Voli 1981; Groenewegen & de Jong 1993) although we know now that this relation breaks down for

<sup>1</sup>produced from the H and  ${}^4\text{He}$  initially present in the star.

stars undergoing HBB (Bloeker & Schoenberner 1991; Lattanzio 1992). Synthetic AGB models have successfully been used to model AGB populations (Groenewegen & de Jong 1993; Marigo et al. 1996) and compute stellar yields (van den Hoek & Groenewegen 1997; Marigo 2001; Izzard et al. 2004). Many of the parameterizations used in synthetic evolution studies are derived from detailed stellar models, such as the growth of the H-exhausted core with time, and as such are only accurate over the range in mass and metallicity of the stellar models they are based upon. An example is provided by van den Hoek & Groenewegen (1997) who compute AGB yields for initial masses between  $0.9$  and  $8M_{\odot}$  whereas the Boothroyd & Sackmann (1988) interpulse-period-core mass relation they use was only derived for stars with initial masses between  $1$  and  $3M_{\odot}$ . What affect this has on the yields is unclear since this relation will affect the number of TPs during the TP-AGB phase and hence the level of chemical enrichment. Dredge-up and HBB affect these relationships but owing to our lack of understanding about these phenomena, there are still considerable uncertainties that affect the detailed computations. Recent improvements in computer power mean that grids of detailed AGB models can now be produced in a reasonable time (Ventura et al. 2002; Karakas et al. 2002; Herwig 2004b) although producing yields from  $N \gtrsim 20$  AGB stars for any given metallicity range is still challenging. For this reason synthetic models are still preferred for some applications.

In an effort to try and quantify the contribution of AGB stars to the production of elements in the Galaxy we have calculated grids of detailed AGB models covering a substantial range in initial mass and metallicity. The aim of this paper is to provide the results of these grids in a format suitable for many applications. We first present the AGB stellar structure in a format useful for comparison to other detailed models, or for use in synthetic AGB algorithms. Second, we provide the stellar yields. These could be useful for different applications including chemical evolution studies, for comparison to the composition of planetary nebulae (PNe) and pre-solar grains. The data are provided in a tabulated format available for download via the internet, where the appropriate reference for these tables is this paper.

These models were previously discussed in detail in Karakas (2003) and in a number of other studies that help to highlight the importance of these models for both detailed and synthetic AGB calculations. These studies include Karakas et al. (2002), Karakas & Lattanzio (2003), Izzard et al. (2004), Lugaro et al. (2004), Karakas et al. (2006b), Lugaro et al. (2007), Izzard et al. (2007) and Karakas et al. (2007). These later studies used the structure models presented here and changed the reaction rates and/or initial abundances to study particular problems e.g. the effect of reaction rate uncertainties on the production of  $^{19}\text{F}$  in AGB stars (Lugaro et al. 2004).

We begin with a brief description of the numerical method.

## 2 The Numerical Method

The numerical method we use has been previously described in detail (e.g. Lugaro et al. 2004; Karakas et al. 2006b). Here we summarize the main points relevant for this study. We compute the structure first and then perform detailed nucleosynthesis calculations.

### 2.1 The Stellar Structure models

The stellar structure models were calculated with the Monash version of the Mount Stromlo Stellar Structure Program; see Frost & Lattanzio (1996) and references therein for details. Mass loss on the first giant branch is included using the Reimer's mass-loss prescription (Reimers 1975, hereafter R75) with the parameter  $\eta = 0.4$ ; on the AGB we use the formulation given by Vassiliadis & Wood (1993, hereafter VW93) in all models unless indicated otherwise. We calculate two models ( $5M_{\odot}$ ,  $Z = 0.02$  and  $Z = 0.0001$ ) using Reimer's mass loss on the AGB with the parameter  $\eta = 3.5$ . We used the solar abundances of Anders & Grevesse (1989) for the  $Z = 0.02$  models. For the  $Z = 0.008$  and  $0.004$  models we used C, N, and O abundances from Russell & Dopita (1992) that are appropriate for stars in the Large and Small Magellanic Clouds where many AGB studies are performed. We assumed scaled-solar abundances for the  $Z = 0.0001$  models.

All models were calculated from the zero-age main sequence to near the end of the TP-AGB phase. For models with initial masses below  $2.5M_{\odot}$  we also evolve the models through the core He-flash. While this is an approximation to the true 3D nature of the core flash (Dearborn et al. 2006), it at least allows us to model the entire evolution of the star self-consistently without resorting to using zero-age horizontal branch models or other techniques to get around this event (see for e.g. Stancliffe et al. 2004).

The occurrence of the TDU and HBB depend critically upon the convection model used (Frost & Lattanzio 1996; Mowlavi 1999; Ventura & D'Antona 2005a) and the method for determining convective borders. We use the standard mixing-length theory (MLT) for convective regions with a mixing-length parameter  $\alpha = l/H_P = 1.75$ , and determine the border by applying the Schwarzschild criterion. Hence we do not include convective overshoot, in the usual sense. Instead we search for a neutral border to the convective zone in the manner described by Lattanzio (1986). This method has been shown to increase the efficiency of the TDU compared to models that strictly use the Schwarzschild criterion (Frost & Lattanzio 1996).

We will not provide a detailed discussion of the uncertainties that affect our models but we refer the interested reader to Frost & Lattanzio (1996), Busso et al. (1999), Goriely & Mowlavi (2000), Ventura & D'Antona (2005a,b)

Table 1: Grids of stellar masses for each  $Z$ , noting if the models experience the core He-flash (CHe), the third dredge-up (TDU), and hot bottom burning (HBB).

mass	$Z = 0.02$	$Z = 0.008$	$Z = 0.004$	$Z = 10^{-4}$
1.0	CHe	CHe	CHe	–
1.25	CHe	CHe	CHe	CHe,TDU
1.5	CHe	CHe	CHe,TDU	–
1.75	CHe	CHe,TDU	CHe,TDU	CHe,TDU
1.9	CHe	CHe,TDU	CHe,TDU	–
2.0	CHe	–	–	TDU
2.1	–	CHe,TDU	–	–
2.25	CHe,TDU	TDU	TDU	TDU
2.5	TDU	TDU	TDU	TDU
3.0	TDU	TDU	TDU	TDU,HBB
3.5	TDU	TDU	TDU	TDU,HBB
4.0	TDU	TDU,HBB	TDU,HBB	TDU, HBB
5.0	TDU,HBB	TDU,HBB	TDU,HBB	TDU,HBB
6.0	TDU,HBB	TDU,HBB	TDU,HBB	TDU,HBB
6.5	TDU,HBB	–	–	–
7.0	–	–	–	TDU,HBB <sup>a</sup>

<sup>a</sup> This model goes through central C-burning and is a super-AGB star.

and Herwig (2005) noting that this is a non-exhaustive list of publications dedicated to discussing uncertainties in the modelling of AGB stars.

## 2.2 Post-processing Nucleosynthesis models

We performed detailed nucleosynthesis calculations using a post-processing code that includes 74 species and time-dependent diffusive mixing in all convective zones (Cannon 1993). The details of the nucleosynthesis network are outlined in Lugaro et al. (2004) but we remind the reader that we include 59 light nuclei and 14 iron-group species. We also add the fictional particle  $g$  to count the number of neutron captures occurring beyond  $^{62}\text{Ni}$  (Lattanzio et al. 1996; Lugaro et al. 2004).

The bulk of the 506 reaction rates are from the REACLIB data tables (Thielemann et al. 1986), based on the 1991 updated version. Some of the proton,  $\alpha$  and neutron capture reaction rates have been updated according to the latest experimental results, see Lugaro et al. (2004) for details.

## 3 The Stellar Models

The mass grid used for each metallicity is shown in Table 1 where we note if the model experienced the core He-flash, TDU and/or HBB. For each model AGB star we present structural information in tabulated form and these tables are available for download from the website [http://www.mso.anu.edu.au/~akarakas/model\\_data/](http://www.mso.anu.edu.au/~akarakas/model_data/). Samples are given in Tables 2 and 3. Data is provided as a function of the TP number as a proxy for time. Each table contains the pulse number, and for that pulse we include the core mass  $M_{\text{core}}$ , the maximum extent of the pulse-driven convection region  $M_{\text{csh}}$ , the maximum duration of the convective pocket  $t_{\text{csh}}$ , the amount of matter dredged into the envelope  $\Delta M_{\text{dredge}}$ , the parameters  $\lambda$  and  $\lambda_{\text{dup}}$  (see below), and the maximum temperature in the He-shell  $T_{\text{Hshell}}$  (measured from the middle of the He-shell which is hotter than the bottom). We include the maximum temperature at the base of the convective envelope  $T_{\text{bce}}$ , and the maximum temperature in the H-shell  $T_{\text{Hshell}}$ ; these were computed over the previous interpulse period. We then include the interpulse period, the total mass (measured at the current TP)  $M_{\text{tot}}$ , the maximum radiated luminosity during the previous interpulse period Max L, and the maximum He-luminosity during the current TP Max LHe. All units are in solar units with the exception of temperatures, that are in kelvin, and all times which are in years.

The TDU efficiency parameter,  $\lambda$ , is usually defined according to  $\lambda = \Delta M_{\text{dredge}}/\Delta M_{\text{h}}$ , where  $\Delta M_{\text{h}}$  is the amount by which the core mass has grown between the present and previous TPs. In our tables we provide  $\lambda$  along with the parameter  $\lambda_{\text{dup}}$ , defined by Goriely & Mowlavi (2000) to be  $\Delta M_{\text{dredge}}/M_{\text{csh}}$ . This quantity is useful for comparison to the results of Goriely & Mowlavi (2000) and also because it provides a measure of the amount of pulse-driven convective mass mixed into the outer envelope. In the study by Goriely & Mowlavi (2000) they assumed a constant value of  $\lambda_{\text{dup}} = 0.1$  whereas we observe this parameter to increase as a function of TP number in models that experience the TDU.

We had originally aimed to evolve each model  $\Delta \log T_{\text{eff}} \sim 0.3$  off the AGB track, to the point where the entire outer envelope of the model had been lost. Owing to convergence difficulties near the tip of the AGB this was only achieved in one case: the  $1M_{\odot}$ ,  $Z = 0.02$  model where mass loss removed the entire outer envelope, leaving the model with a final remnant mass of  $0.573M_{\odot}$  and on the white-dwarf cooling track with a final  $\log T_{\text{eff}} = 4.118$ . The low-mass models ( $M < 2M_{\odot}$ ) lost most of their outer envelopes, even if they did not leave the AGB track completely according to the definition above. For most of these models the remaining envelope mass was small, much less than  $0.1M_{\odot}$  and we would not expect further TPs on the AGB. For the more massive models the remaining envelope mass was large enough that further TPs would probably occur if we could evolve the models further along the AGB track. In all cases however the luminosity-driven superwind phase had started and the envelope mass was being reduced at a rapid rate, at a few  $\times 10^{-5} M_{\odot} \text{ year}^{-1}$ . HBB had ceased to operate in all models; this occurred once the envelope mass was reduced below about  $\sim 1.5M_{\odot}$ . In §4 we discuss how we estimated the number of remaining TPs and the contribution of these pulses to the chemical enrichment of the model star.

The convergence difficulties mostly occurred during the start of the final TDU phase, after the TP has peaked in He-luminosity. The reasons for the convergence problems are unclear but they are not associated with small values of the gas pressure to total pressure,  $\beta$ , since previous dredge-up episodes occur without problem for similar values of  $\beta$ . The convergence problems are sometimes associated with a rapid drop in the temperature at the base of the convective envelope and an increase in the stellar radius. Higher metallicity models, at a given initial mass, experience convergence difficulties earlier (i.e. at a larger envelope mass) than models of lower metallicity. This may indicate that the input physics, notably the opacities, are related to the problem. A thorough investigation into the cause of the convergence difficulties is required.

Two models require a special mention and these are the  $6$  and  $7M_{\odot}$ ,  $Z = 0.0001$  models. The  $6M_{\odot}$  model was evolved through more than 100 TPs but by the time we ended the computation, little envelope mass had been removed, the superwind phase had not been reached and HBB was actively changing the composition of the outer envelope. For this model we estimate that another 100 could possibly occur when using the Vassiliadis & Wood (1993) mass-loss prescription. We do not attempt to estimate the contribution from the remaining TPs owing to the complication caused by active HBB; see Izzard et al. (2006) for the difficulties associated with this. The  $7M_{\odot}$  model went through degenerate central carbon burning before ascending the TP-AGB phase. For this model we only computed 12 TPs before we ended the computation. We point out that it is unclear if this model would end its life as a massive ONe white dwarf or it would reach the Chandrasekhar limiting mass and explode as a low-mass Type II supernova. At the end of the computation, the final core mass was  $1.126M_{\odot}$  and with inefficient TDU and a low mass-loss rate we suspect it would explode as a low-mass Type II supernova but further study is required to determine the final fate of this model.

In Tables 2 and 3 we present the results for the  $3M_{\odot}$ ,  $Z = 0.02$  model, to show an example of the tables available. Note that these data are given as one table for each mass and  $Z$  in the on-line version. For the case shown the TDU begins at the 10<sup>th</sup> TP when the core mass reaches  $0.62M_{\odot}$ . Adding up the  $\Delta M_{\text{dredge}}$  for each pulse gives a total of  $0.0787M_{\odot}$  core material that is added to the envelope over the course of the TP-AGB phase. This model does not experience HBB and that can be seen by inspection of Table 3 where the maximum temperature at the base of the convective envelope during the interpulse does not exceed  $10^7$  K. Other interesting comparisons can be made by considering the evolution of the interpulse period as a function of the core mass. From the data presented in Table 3 we observe an initial increase followed by slow decrease. We can compare to the core mass–interpulse period relations given in Boothroyd & Sackmann (1988) or Wagenhuber & Groenewegen (1998) at the final core mass of the model,  $0.68M_{\odot}$ . The first relation gives a value of  $3.47 \times 10^4$  years and the second  $3.73 \times 10^4$  years. Both of these values are significantly smaller than the value that comes out of the detailed computation of  $5.47 \times 10^4$  years. Hence synthetic AGB simulations using either of these relations would result in many more TPs during the TP-AGB than we predict and hence more TDU episodes and a greater level of chemical enrichment.

### 3.1 The Third Dredge-up and HBB

Owing mostly to the operation of TDU episodes AGB stars are important for enriching the composition of the interstellar medium (ISM). Observational evidence suggests that the TDU occurs in stars as low as  $\sim 1.2M_{\odot}$  at solar metallicity and in the LMC (Frogel et al. 1990; Wallerstein & Knapp 1998) and at  $\sim 1M_{\odot}$  in the SMC (Frogel et al. 1990). An examination of the tables presented above show that the minimum mass for the TDU at solar metallicity is  $2.25M_{\odot}$ , and  $1.5M_{\odot}$  at the metallicities appropriate for the LMC ( $Z = 0.008$ ) and SMC ( $Z = 0.004$ ). In Karakas et al. (2002) we discussed in detail how these models do not predict enough TDU at small enough core masses to account for the observations. The recent analysis of infra-red data by Guandalini et al. (2006) suggests that the minimum mass of stars experiencing the TDU has previously been greatly under-estimated, owing to incorrect estimates of bolometric magnitudes. However if the study of Stancliffe et al. (2005) is anything to go on there is still a requirement for more efficient TDU in low-mass low-metallicity stars than we predict.

Massive AGB stars that experience HBB are one of the favoured sites of the abundance anomalies observed in galactic globular cluster stars (Yong et al. 2003; Gratton et al. 2004), even if problems persist in comparisons between the model predictions and the observed abundance trends (Denissenkov & Herwig 2003; Fenner et al. 2004; Ventura & D’Antona 2005b; Karakas et al. 2006a). Observations of stars experiencing HBB have mostly

come from the LMC and SMC (Wood et al. 1983; Plez et al. 1993), with some observations of stars in our Galaxy (Garcia-Hernandez et al. 2006, 2007). These observations indicate that most luminous AGB stars have an O-rich composition (where  $C/O < 1$ ) with a low  $^{12}C/^{13}C$  ratio, and that many are also rich in Li (Smith & Lambert 1990), and in elements produced by the slow-neutron capture process. Observations by McSaveney et al. (2007) have shown that two bright O-rich AGB stars are rich in nitrogen and depleted in carbon. These observations are the first observational confirmation of the long-predicted production of primary nitrogen by the combination of TDU and HBB in intermediate-mass AGB stars.

## 4 The Stellar Yields

The stellar yields can be downloaded from the website: [http://www.mso.anu.edu.au/~akarakas/stellar\\_yields/](http://www.mso.anu.edu.au/~akarakas/stellar_yields/). We present the stellar yields in two ways. The first method presents the yields and abundances in the wind integrated over the entire stellar lifetime and these are suitable for use in e.g. galactic chemical evolution studies. An example is given in Table 5. Each of the tables contain the following: 1) the nuclear species  $i$ , 2) the atomic mass  $A(i)$ , 3) the nett stellar yield, defined below, 4) the amount of species  $i$  in the wind lost from the star  $\text{mass}(i)_{\text{lost}} (M_{\odot})$ , 5) the amount of  $i$  that would initially have been present in the wind  $\text{mass}(i)_0 (M_{\odot})$ . The quantity  $\text{mass}(i)_0$  is simply the mass expelled during the stellar lifetime multiplied by the initial abundance. We next include 6) the average mass fraction of  $i$  in the wind  $\langle X(i) \rangle$ , 7) the initial mass fraction  $X_0(i)$  and 8) the production factor  $f$  defined by  $\log[\langle X(i) \rangle / X_0(i)]$ . Note that in Table 5 the production factor has simply been labelled  $f$  whereas the definition is provided in the header of the on-line tables. This last quantity  $f$  is useful for comparison to authors who present their results in a similar way (see Table 4 from Herwig 2004b) as well as for comparison to derived abundances from stars, where for e.g. an  $f \approx 0.2$  would indicate an increase of that species by 0.2 dex at the surface.

The definition of the yield that we use is given by the following expression

$$M_i = \int_0^{\tau} [X(i) - X_0(k)] \frac{dM}{dt} dt, \quad (1)$$

where  $M_i$  is the yield of species  $i$  (in solar masses),  $dM/dt$  is the current mass-loss rate,  $X(i)$  and  $X_0(i)$  refer to the current and initial mass fraction of species  $i$ , and  $\tau$  is the total lifetime of the stellar model. The yield can be negative, in the case where the element is destroyed, and positive if it is produced. We also present the total amount of  $i$  (in  $M_{\odot}$ ) expelled into the ISM, noting that this value is always positive.

It was previously discussed that some of the models do not lose their entire outer envelopes during the TP-AGB evolution owing to convergence difficulties near the tip of the AGB. This may be important for the stellar yields because, depending on the amount of remaining envelope, these models may experience further TPs and TDU episodes. Even one more TDU episode could significantly alter the surface abundances at this stage because the envelope mass is small leading to less dilution. The affect on the stellar yields is probably smaller because this quantity is integrated over the entire stellar lifetime.

For each model we estimate the number of remaining TPs; this is shown in Table 4 along with the TDU efficiency parameter from the last computed TP,  $\lambda_f$ . Models not included in this table have small enough envelope masses that we estimate that no further TPs would take place. For the models in Table 4 we present two sets of stellar yields, one with no contribution from these extra pulses; this is where we remove the envelope at its given composition and assume that  $\lambda = 0$  during remaining pulses. The other set of yields were computed using a constant value of  $\lambda$  for the remaining TPs. This latter set are our “standard” set and we recommend these be used. The set with  $\lambda = 0$  are useful for exploring model uncertainties.

From inspection of Table 4 an example of a model where remaining TPs might affect the yields is the  $6M_{\odot}$ ,  $Z = 0.02$  model where we estimate that 5 more TPs could occur. The magnitude of the change to the surface composition from these final TPs depends on one big unknown: The behaviour of  $\lambda$  with decreasing envelope mass. Detailed stellar models suggests that  $\lambda$  decreases with decreasing envelope mass (Straniero et al. 1997; Karakas et al. 2002, and data presented here) but Stancliffe & Jeffery (2007) find results to the contrary and instead suggest that there is no reduction in  $\lambda$ , at least for the  $1.5M_{\odot}$  models discussed in that paper.

In Table 5 we present a set of stellar yields for the  $3M_{\odot}$ ,  $Z = 0.02$  model. From Table 4 we estimate that one more TP would occur for this model and the yields presented here include this final TP. In Table 5 we only show results for the 39 nuclear species that had stellar yields with mean magnitudes greater than  $\sim 10^{-10}$  and hence neglect many short-lived unstable isotopes that are included in the nucleosynthesis network as well as in the tables that are available for download. Using this criterion we have included results for the important radio-nuclides  $^{26}\text{Al}$  and  $^{60}\text{Fe}$ , noting that we set the production factors to be zero for these models owing to an initial zero abundance.

For the  $3M_{\odot}$ ,  $Z = 0.02$  model we estimate that the last TP will occur when the total stellar mass was  $\sim 1.35M_{\odot}$  and the envelope  $\sim 0.66M_{\odot}$ . From inspection of Table 3 it is clear that this last TDU episode occurs at a much smaller envelope mass than all previous mixing episodes, where  $M_{\text{env}} \gtrsim 2M_{\odot}$ . Consequently the change to the surface abundances was larger and this can be seen in Fig. 1 where we show the evolution of the C/O ratio at the surface. To see what effect this last TDU episode has on the stellar yields we compare the nett yield of  $^{12}\text{C}$ . Without this final TDU episode the nett yield of  $^{12}\text{C}$  is  $1.354 \times 10^{-2} M_{\odot}$  whereas with that final mixing event the

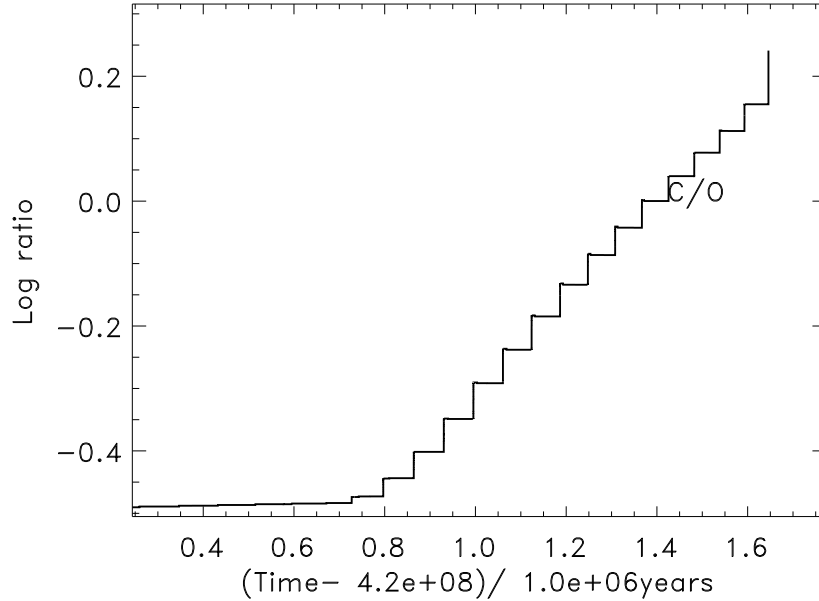


Figure 1: The evolution of the C/O ratio at the surface during the TP-AGB phase of the  $3M_{\odot}$ ,  $Z = 0.02$ . The final C/O ratio for this model is 1.43.

yield is  $1.496 \times 10^{-2} M_{\odot}$ , an increase of about 11%. On the other hand the change to the final surface abundance of  $^{12}\text{C}$  is about 20%.

Before we move on it is important to discuss the effect of the initial mass on the degree of chemical enrichment. It was mentioned above that the  $6M_{\odot}$   $Z = 0.02$  model had an extra 5 TPs left, given the final envelope mass of  $1.53M_{\odot}$  from the end of the detailed calculation. While it would seem obvious that a greater number of remaining TPs would lead to a larger enrichment of the envelope, we need to remember that the He-intershell is about a factor of 10 smaller in an intermediate-mass AGB star. For this reason the amount of matter dredged into the envelope at each TDU episode is smaller, regardless of the value of  $\lambda$ . This can be seen from inspection of the tables given in §3 where the maximum mass of the pulse-driven pocket (approximately equal to the mass of the intershell at the TP) is  $0.016M_{\odot}$  for the  $3M_{\odot}$ ,  $Z = 0.02$  model whereas this value is reduced to  $0.0033M_{\odot}$  in the  $6M_{\odot}$ ,  $Z = 0.02$  case. The mass of the envelope in the  $6M_{\odot}$  model was also larger at each TDU episode resulting in more dilution of dredged-up material. For this massive AGB model, the final surface abundance of  $^{12}\text{C}$  increased by about 26% as a consequence of the 5 extra TPs, only marginally more than the 20% increase from only **one** TP for the  $3M_{\odot}$ ,  $Z = 0.02$  case, as discussed above.

The stellar yields that we present here may be slightly different to those presented in Karakas (2003) because we have improved the synthetic AGB algorithm used to estimate the surface enrichment from the final TPs. The main improvement is taking intershell compositions for the last TP for all 74 species from the detailed stellar models. Previously we estimated the intershell compositions for about 15 species (e.g.  $^4\text{He}$ ,  $^{12}\text{C}$ ,  $^{16}\text{O}$ ,  $^{22}\text{Ne}$  etc) and assumed the rest did not change. We also did not have intershell compositions for each mass and  $Z$ , so in some cases we assumed that compositions appropriate for e.g. the  $3M_{\odot}$ ,  $Z = 0.004$  model were appropriate for the  $2.5$  and  $3.5M_{\odot}$  models of the same  $Z$ . We have also improved the input data required for the synthetic code, e.g. the final computed interpulse period and TDU efficiency. These improvements change the final remnant mass (at least slightly) and this also results in slight changes to the stellar yields.

## 4.1 Planetary nebulae

After the outer envelope has been ejected the stars evolve through the brief post-AGB and planetary nebula (PN) phases of the Hertzsprung-Russell diagram (van Winckel 2003). The glowing gas of the nebula is the remnant of the outer convective envelope of the progenitor AGB star and hence its composition should reflect the nucleosynthesis that took place during the final few TPs on the TP-AGB.

Planetary nebulae are important because their compositions can be determined fairly accurately (at least for some species); because they are bright, abundances can be derived from PNe as far away as M31, and because the gas is ionized by UV photons we obtain information about elements normally very difficult to study, in particular

the noble gases He, Ne, Ar, as well as C, N, O (Kaler 1978; Henry 1989; Dopita et al. 1997; Stanghellini et al. 2000). Abundances of heavy elements synthesized by the *s* process including Ge, Se, Kr, Xe Br and Ba (Sterling et al. 2002; Sterling & Dinerstein 2007; Sharpee et al. 2007) are also observed to be enhanced in some nebulae. Owing to the importance of PNe abundances we have included stellar yields for PNe in particular. These yields are the abundance by number in the matter lost from the star from the final two TPs and as such are good for comparison to the composition of the nebular gas for PNe in the Galaxy, LMC and SMC. We have included PN yields for the low-metallicity  $Z = 0.0001$  models but few (if any) PN around today are expected to have evolved from such a low-metallicity population of stars. PNe in the Milky Way Galaxy are predominantly found in the disk with oxygen abundances<sup>2</sup> in the range  $7.73 \lesssim \log \epsilon(\text{O}) \lesssim 9.09$  (Stanghellini et al. 2006) compared to the solar value of 8.66 (Asplund et al. 2005). Only a few PN have been found in the halo and there are only a handful ( $N \sim 12$ ) known that are defined to be metal-poor, with oxygen abundances less than a factor of 4 below solar (Dinerstein et al. 2003).

In Table 6 we show an example of the yields available for a PN originating from a  $3M_{\odot}$  progenitor of solar composition. As for the yields presented previously we compute two sets for models with synthetic TPs and for this case we show the PN set with the final synthetic TP included. The first entry in each on-line table is the amount of matter expelled during the last two TPs, here we include this value in the table caption. The columns contain the species  $i$ , the atomic weight  $A(i)$ , followed by the nett yield, the mass lost, the initial mass fraction, and the average mass fraction integrated over the final two TPs. The next quantity is the abundance (by number) of the matter lost in the wind over the final two TPs, compared to the number of hydrogen atoms,  $N_i/N_{\text{H}}$ . This quantity is often used in the literature in the form  $\log \epsilon = \log(N_i/N_{\text{H}}) + 12$ .

Comparing results for  $^{12}\text{C}$  from Table 6 to Table 5 we see that the nett yield is lower in the PN table by  $\sim 27\%$ , this is consequence of less matter being lost in the final two pulses than over the whole lifetime, even though the average  $^{12}\text{C}$  abundance is higher by  $\sim 8\%$ . Remember that our definition of a stellar yield defined in Equation 1 essentially subtracts the amount of  $i$  in the wind lost from the star (i.e.  $\approx M_{\text{lost}}^{\text{total}} \times \langle X(i) \rangle$ ), by the amount of  $i$  that would have been initially present in that wind (i.e.  $M_{\text{lost}}^{\text{total}} \times X_0(i)$ ). Note that the  $3M_{\odot}$ ,  $Z = 0.02$  model lost  $1.508M_{\odot}$  over the last two TPs compared to  $3.0 - M_{\text{f}} = 2.318M_{\odot}$  over the entire lifetime (see Table 4 for the final mass).

That the yield difference was not larger is a consequence of the VW93 mass-loss prescription. This prescription ensures that the mass-loss rate is low until the superwind begins at which stage most of the envelope is lost in a few TPs. For the  $5M_{\odot}$ ,  $Z = 0.02$  model we computed an evolutionary sequence with the R75 mass-loss law with  $\eta = 3.5$ . For this model the nett PN yield of  $^{12}\text{C}$  is 3.42 times lower than the total yield, compared to 1.68 times lower for the VW93 case. The total amount of matter expelled is  $0.75M_{\odot}$  and  $0.58M_{\odot}$ , for the VW93 and R75 cases, respectively. Note that the average  $^{12}\text{C}$  abundance in the wind expelled over the last two TPs increased in both models, where the R75 model saw a 66% increase compared to 63% for the VW93 case.

## 4.2 Limitations of the current models

We discussed in the previous section that we did not include a partial mixing zone at the deepest extent of each TDU episode to produce a  $^{13}\text{C}$  pocket. This can be considered a limitation since the neutrons produced by the  $^{13}\text{C}(\alpha, n)^{16}\text{O}$  reaction can affect the composition of the He-shell. However the light elements (hydrogen through to phosphorous) are generally not significantly altered by neutron captures, at least at solar metallicity. There are exceptions to this, including the nucleosynthesis of  $^{19}\text{F}$  that requires the operation of the  $^{13}\text{C}$  neutron source in low-mass AGB stars of  $\sim 3M_{\odot}$  (Jorissen et al. 1992; Lugaro et al. 2004). Sodium, the magnesium and silicon isotopes, and  $^{31}\text{P}$  are affected by neutron captures during the TP where neutrons are released by the  $^{22}\text{Ne}$  source at higher neutron densities ( $\sim 10^{10} \text{ cm}^{-3}$ ), noting we include this in our computations. Neutron captures will impact more significantly on light-element nucleosynthesis in more massive or lower metallicity models, as pointed out by Herwig (2004a,b).

One limitation of our models, at least in terms of their use for galactic chemical evolution studies, are the initial C, N and O abundances used for the  $Z = 0.008$  and  $0.004$  models. These are not scaled solar but reflect the composition of the LMC and SMC, respectively. Our models are therefore very useful for comparing to the composition of AGB stars and PN in the Large and Small Magellanic Clouds, which was their intended use, but one must be careful when using the C, N and O yields for comparison to populations that have a similar  $[\text{Fe}/\text{H}]$  content of the Clouds but a different chemical history. We have started to compute yields assuming a scaled-solar composition for those metallicities and these will be available in a future publication.

Another limitation is that our lowest metallicity models are  $Z = 10^{-4}$  whereas there are many new discoveries of low-mass halo stars with  $[\text{Fe}/\text{H}] \lesssim -3$  (Beers & Christlieb 2005), some of which could have been polluted by a former AGB companion. We do not intend to compute AGB models with such low metallicities in the future but we refer the reader to Simon Campbell's models (Campbell 2007). Besides that  $7M_{\odot}$ ,  $Z = 0.0001$  super-AGB star we do not compute models for any more of these objects. Yields for these stars should be available in the future (Doherty, Lattanzio & Siess, in preparation), noting that models of these stars are proving to be even more challenging than for CO-core AGB models (Siess 2006).

<sup>2</sup>used as a proxy for metallicities because Fe is difficult to measure owing to condensation into dust.

We do not include the effect of extra-mixing processes into our computations, and by this we mean mixing events beyond those predicted to occur by standard models such as ours e.g. the first and second dredge-up, the TDU and HBB. Observations suggest that extra-mixing processes reduce the  $^{12}\text{C}/^{13}\text{C}$  ratio in low-mass ( $m \lesssim 2M_{\odot}$ ) red giant stars below that predicted by standard models (Charbonnel 1994). Observations of AGB stars and pre-solar grain analysis indicate that a similar type of extra-mixing occurs in low-mass AGB stars (Boothroyd et al. 1995; Abia & Isern 1997; Busso et al. 1999; Nollett et al. 2003). While the physical mechanism for the extra-mixing is unknown<sup>3</sup> it is commonly thought to be rotation (e.g. Palacios et al. 2006), although we also refer to the mixing recently discovered by (Eggleton et al. 2006) and investigated further by Eggleton et al. (2007) and (Charbonnel & Zahn 2007).

### 4.3 Comparison with other yields

In this section we provide a brief comparison of our yields to other authors. Karakas (2003) and Izzard et al. (2004) provided a detailed comparison of Izzard's synthetic yields to our detailed models (which his synthetic AGB algorithm is based upon), and to those from other synthetic AGB models (van den Hoek & Groenewegen 1997; Marigo 2001). We do not repeat that discussion here but instead we present diagrams in Figs. 2 to 11, and we discuss results for  $^{12}\text{C}$  and  $^{14}\text{N}$ . In Fig. 4 we show the stellar yields of  $^{12}\text{C}$ , a nuclei representative of low-mass AGB evolution where the effects of TDU episodes are important. In Fig. 6 we show the yields of  $^{14}\text{N}$ , a nuclei that tracks HBB nucleosynthesis. In each figure we show the results for three metallicities,  $Z = 0.02, 0.008$  and  $0.004$  compared to yields from synthetic AGB models, see the figure captions for more details. In each figure we have weighted the yields by the three-component IMF of Kroupa et al. (1993) such that

$$y_i = \frac{dY}{dM} = \xi(M_0) M_i, \quad (2)$$

where  $y_i$  is the weighted yield and  $M_i$  is given by equation 1.

From the Figs. 4 and 6 we see that our yields are almost the same as Izzard et al. (2004) owing to the fact that these synthetic models were tweaked to match our results. Our yields are similar in behaviour to those of Marigo (2001), although because her models experience deeper TDU at a lower core mass, the yields of He-shell material e.g.  $^4\text{He}$ ,  $^{12}\text{C}$  are higher. We notice significant differences with van den Hoek & Groenewegen (1997) especially in regards to  $^{14}\text{N}$ . This is owing to their simplistic treatment of HBB nucleosynthesis which under-predicts the amount of CNO cycling compared to the other computations. Stancliffe & Jeffery (2007) provided a detailed comparison between yields from  $1.5M_{\odot}$  models computed with the STARS code to our yields, with the summary that their models experience deeper TDU and hence go in a similar direction to Marigo's, that is larger yields of material that is dredged from the He-burning shell.

In Fig. 8 we show the (unweighted) yields of  $^{15}\text{N}$  and  $^{19}\text{F}$  as a function of the initial mass and metallicity. In this figure we include the  $Z = 10^{-4}$  to show the effect of lower metallicity stellar evolution on the yields. The maximum  $^{19}\text{F}$  yield is pushed to lower mass, owing to a higher He-burning shell and deeper TDU. The yields of  $^{15}\text{N}$  are negative, indicating this isotope is destroyed, and scale with metallicity except in the intermediate-mass  $Z = 10^{-4}$  models, where we find that  $^{15}\text{N}$  is produced. This is as a result of breakout from the  $^{14}\text{N}(p, \gamma)^{15}\text{O}$  reaction at the temperatures and densities of HBB in these lower metallicity models. The production of  $^{15}\text{N}$  at lower metallicities may have important consequences for the evolution of  $^{15}\text{N}$  in the interstellar medium, especially since AGB stars are not considered producers of this rare isotope.

We compare the  $Z = 10^{-4}$  models to the AGB models of Herwig (2004b) of the same metallicity. This comparison is made easier by the fact that both sets of models assumed a scaled-solar composition. Different mass loss was assumed where we used VW93 mass loss and Herwig applied the Blöcker (1995) prescription with the parameter  $\eta_B = 0.1$ , that resulted in more rapid mass loss than we observed. This can be demonstrated by considering the  $2M_{\odot}$ ,  $Z = 10^{-4}$  model as an example. Our  $2M_{\odot}$  calculation experienced 26 TPs compared to 7 for Herwig's model. Even though the maximum amount of matter dredged into the envelope at any one TP was almost the same ( $1.112 \times 10^{-2}$  compared with Herwig's  $1.171 \times 10^{-2} M_{\odot}$ ), the total amount of material dredged into the envelope over the whole TP-AGB was much larger in our case ( $0.2183 M_{\odot}$ ) compared to Herwig's model ( $5.038 \times 10^{-2} M_{\odot}$ ). For this reason our yields and average surface mass fractions are, in general, larger. The average abundance of  $^{12}\text{C}$  in the wind of our model was  $\sim 2$  times larger, of  $^{22}\text{Ne}$  13 times larger and of  $^{23}\text{Na}$  40 times larger. However the average abundance of  $^{16}\text{O}$  was about 8 times larger in Herwig's model. These differences can be attributed to 1) more TPs in our model, leading to more TDU episodes and hotter nucleosynthesis conditions in the He-shell, and 2) different intershell compositions caused by diffusive convective overshoot used in the Herwig model. Overshoot applied to the border at the base of the convective pocket during a TP mixes some CO core matter into the intershell, resulting in increased  $^{12}\text{C}$  and  $^{16}\text{O}$  abundances. These yields differences are similar for all masses in the range  $2 - 6M_{\odot}$ , where the magnitude of the difference increases with increasing mass owing to the greater number of TPs experienced by our intermediate mass models (4, 5 and  $6M_{\odot}$ ).

<sup>3</sup>and this is the main reason why we do not include it! Another reason being that it is essential to have standard models to compare with before testing new physics.



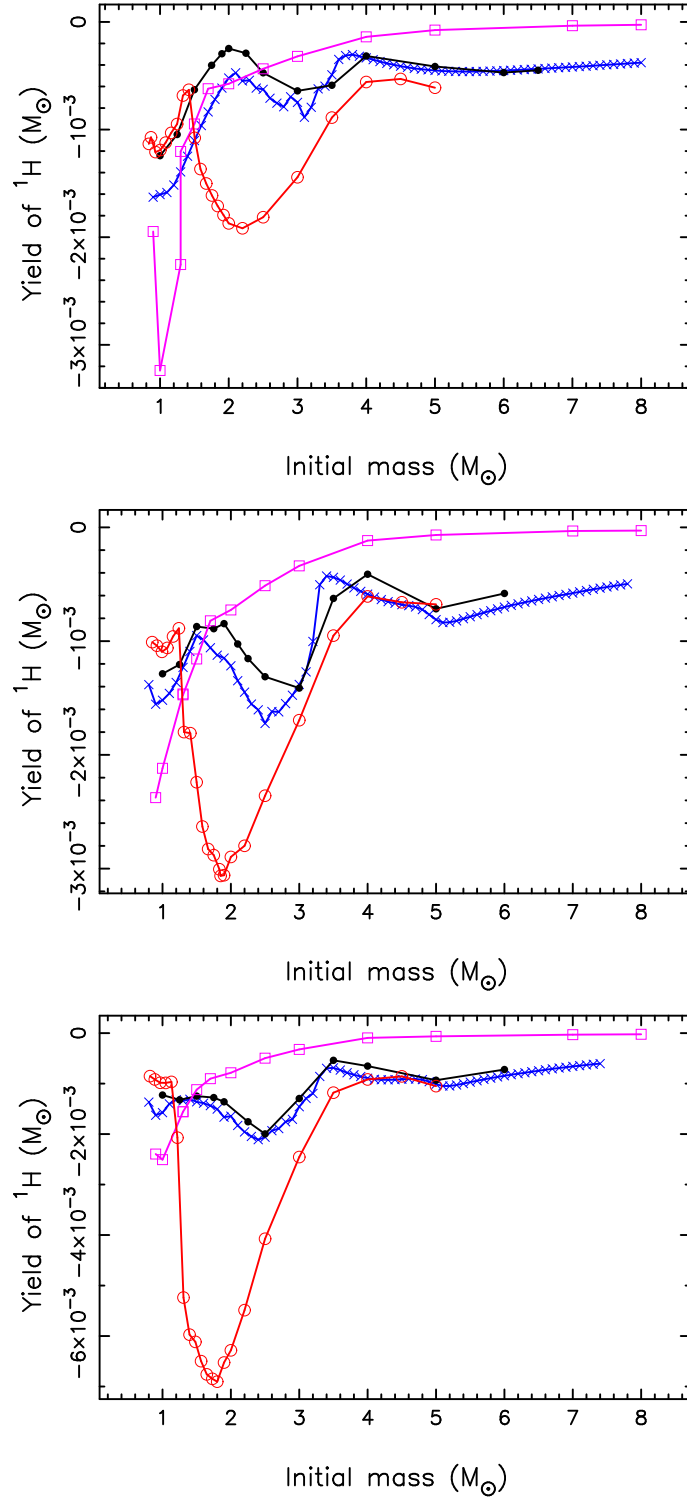


Figure 2: Weighted yield of  $^1\text{H}$  as a function of the initial mass for the  $Z = 0.02$  (top), the  $Z = 0.008$  (middle) and the  $Z = 0.004$  models (bottom). We show results from our calculations (black solid points), van den Hoek & Groenewegen (1997) (open magenta squares), Forestini & Charbonnel (1997) (solid green squares), Marigo (2001) (open red circles), Ventura et al. (2002) (solid aqua triangles) and Izzard et al. (2004) (blue crosses). Forestini & Charbonnel (1997) and Ventura et al. (2002) do not provide yields for  $Z = 0.008$  and cover a narrower mass range, between 3 and 6  $M_\odot$ .

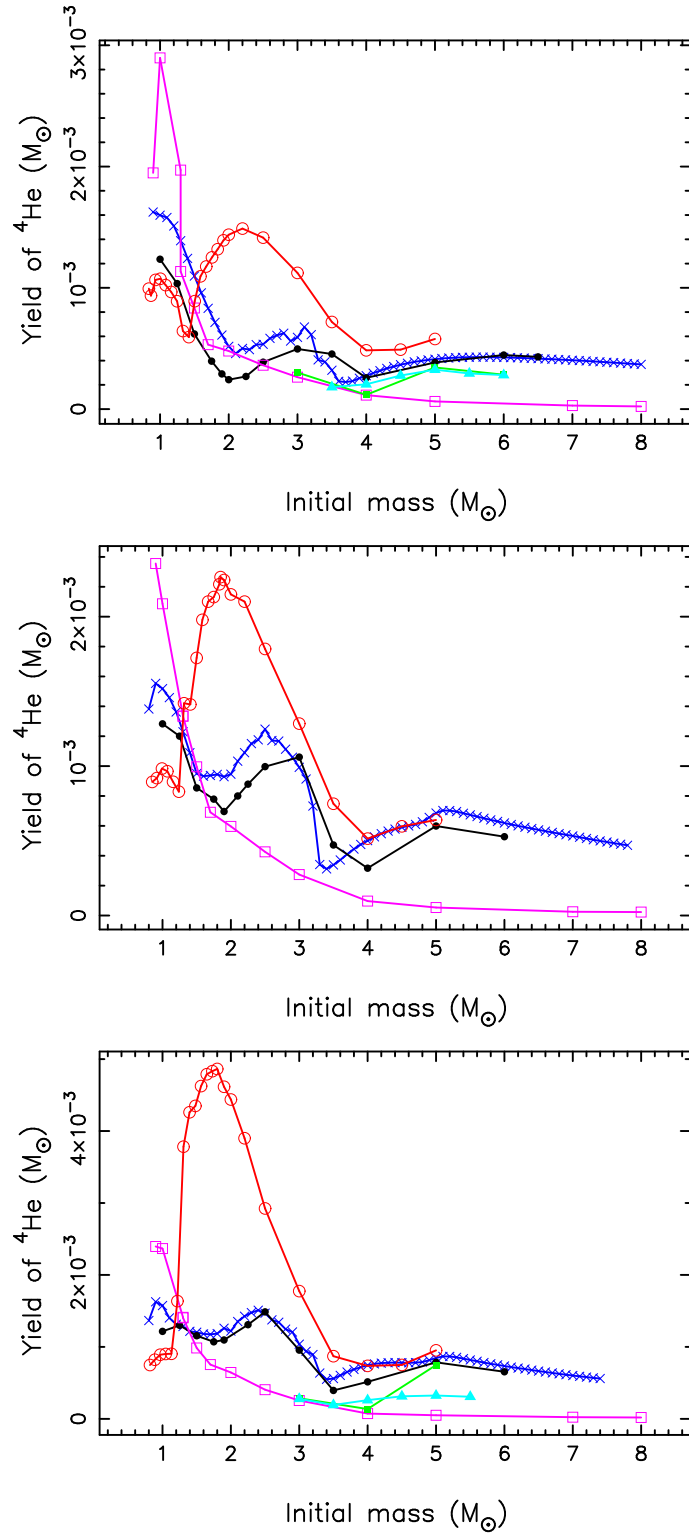


Figure 3: Weighted yield of  ${}^4\text{He}$  as a function of the initial mass for the  $Z = 0.02$  (top), the  $Z = 0.008$  (middle) and the  $Z = 0.004$  models (bottom). Symbols are the same as in Fig. 2.

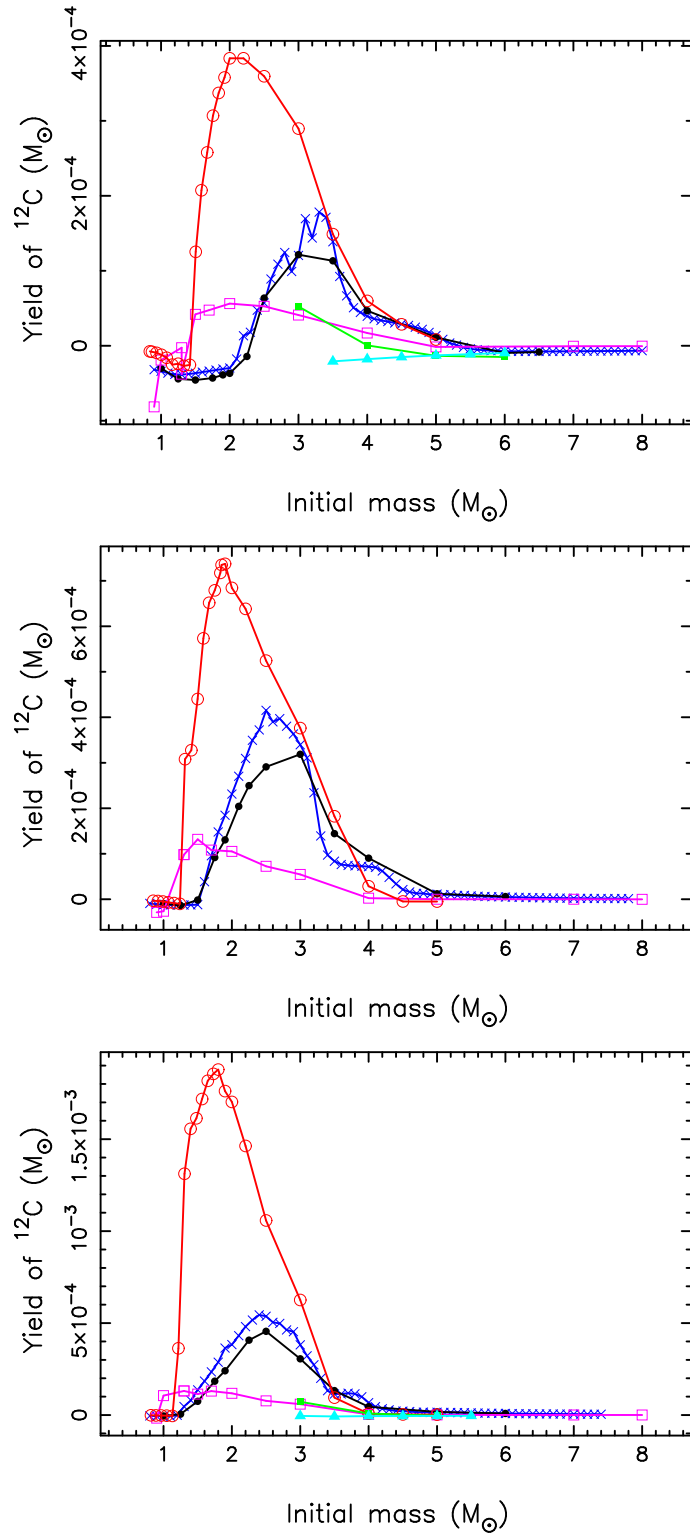


Figure 4: Weighted yield of  $^{12}\text{C}$  as a function of the initial mass for the  $Z = 0.02$  (top), the  $Z = 0.008$  (middle) and the  $Z = 0.004$  models (bottom). Symbols are the same as in Fig. 2.

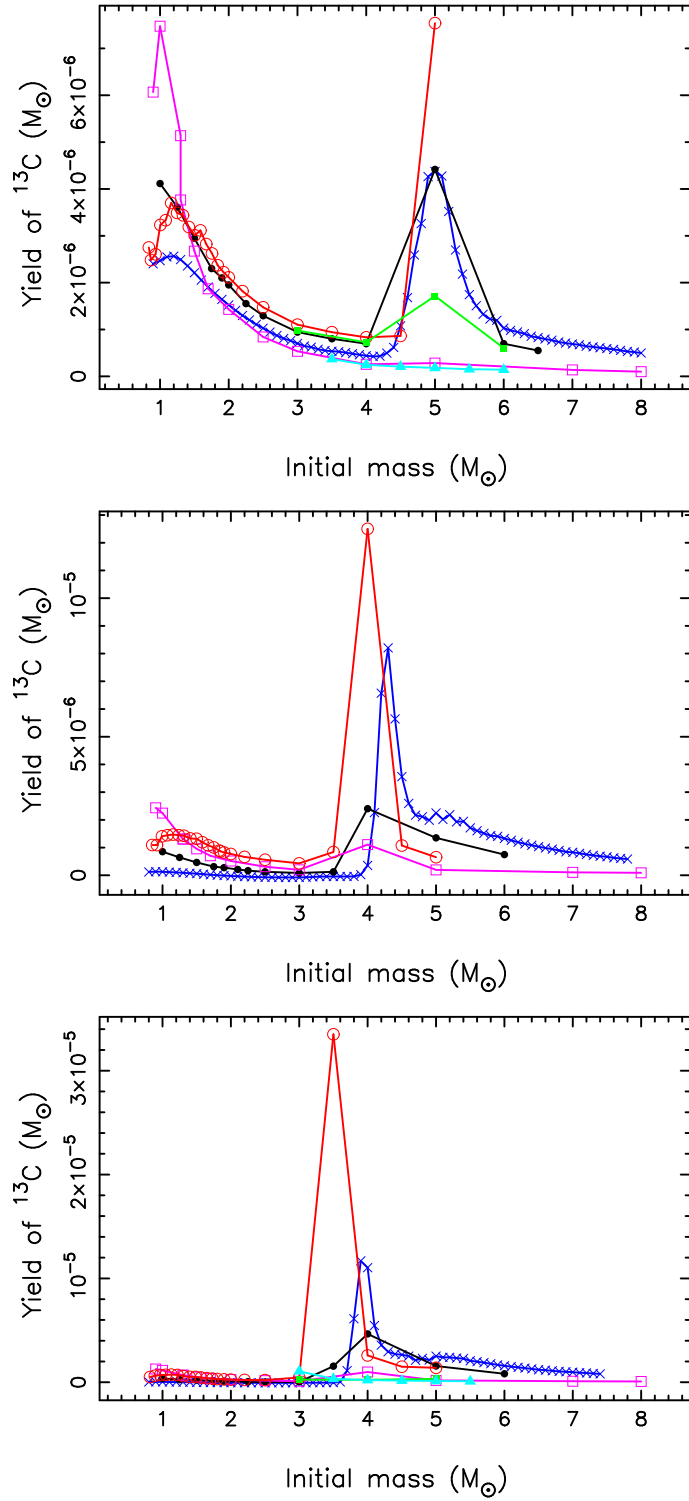


Figure 5: Weighted yield of  $^{13}\text{C}$  as a function of the initial mass for the  $Z = 0.02$  (top), the  $Z = 0.008$  (middle) and the  $Z = 0.004$  models (bottom). Symbols are the same as in Fig. 2.

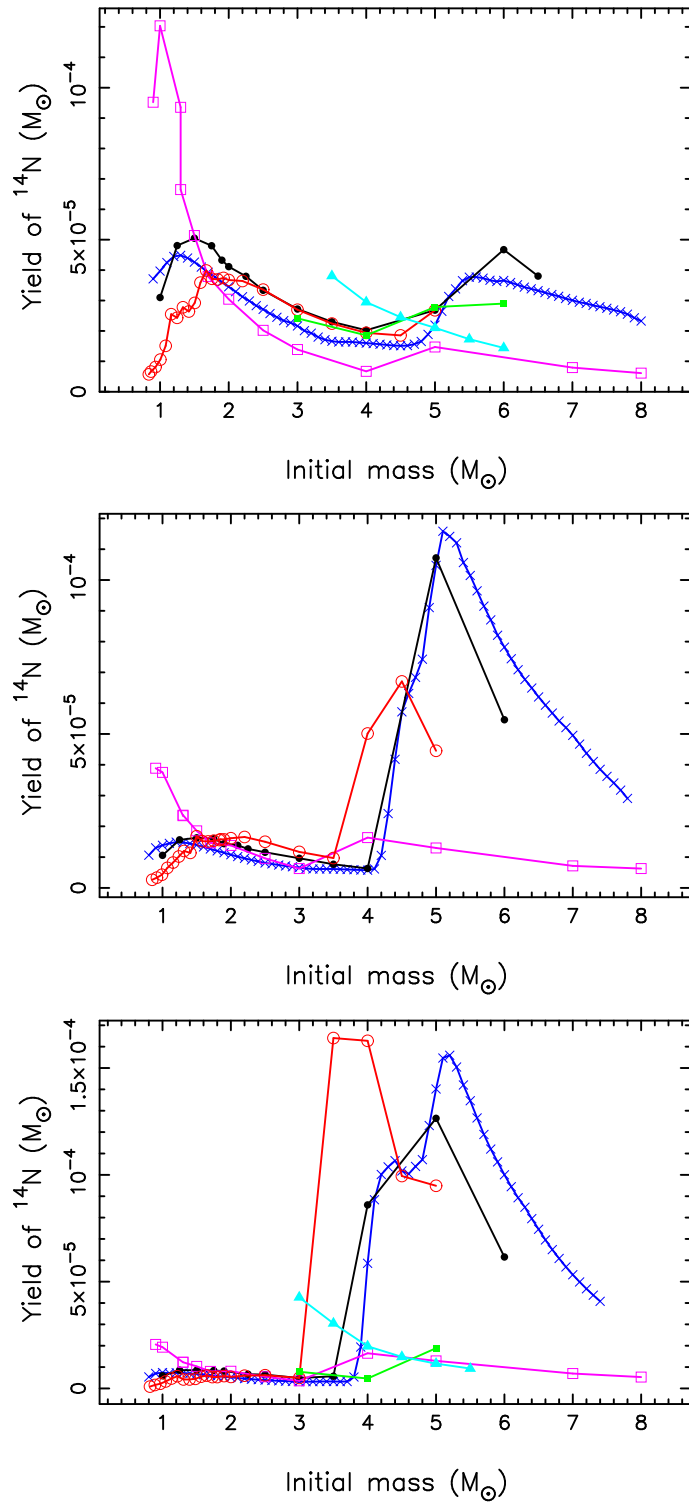


Figure 6: Weighted yield of  $^{14}\text{N}$  as a function of the initial mass for the  $Z = 0.02$  (top), the  $Z = 0.008$  (middle) and the  $Z = 0.004$  models (bottom). Symbols are the same as in Fig. 2.

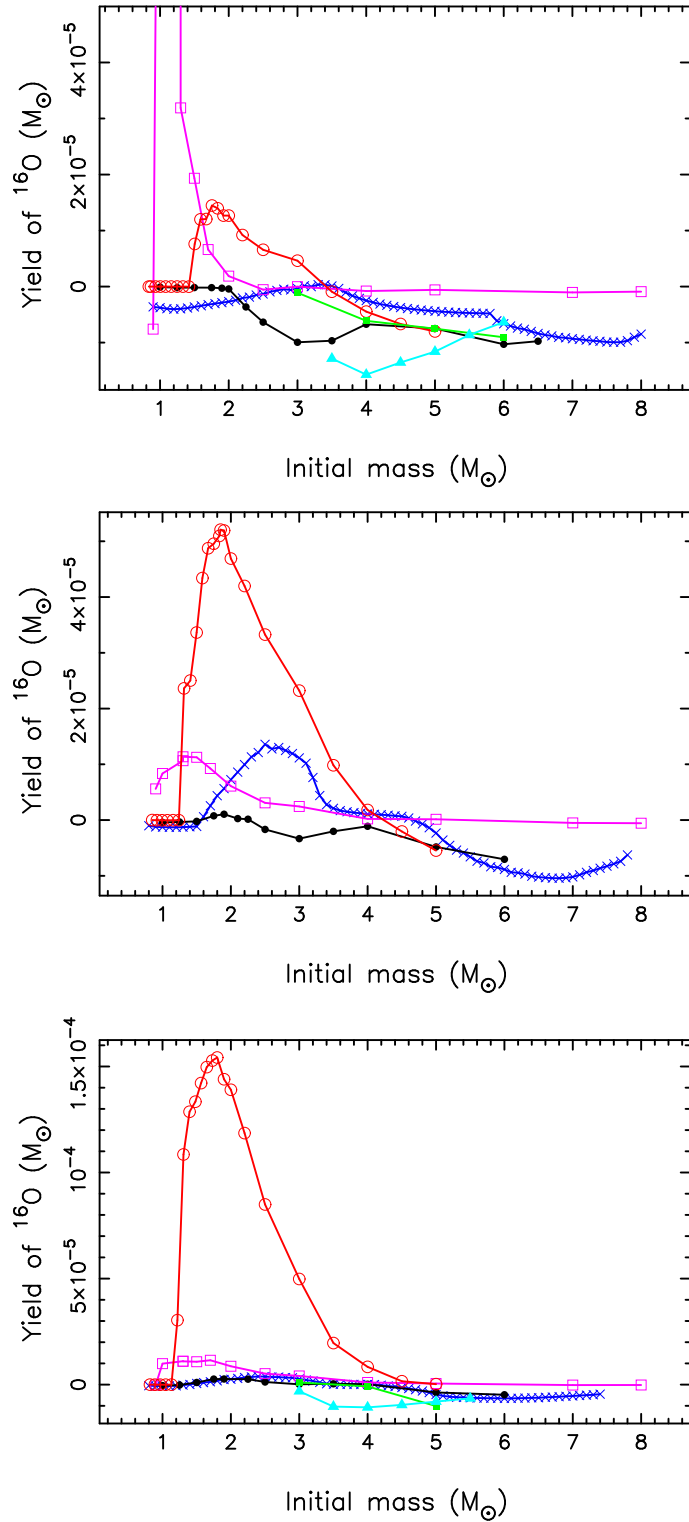


Figure 7: Weighted yield of  $^{16}\text{O}$  as a function of the initial mass for the  $Z = 0.02$  (top), the  $Z = 0.008$  (middle) and the  $Z = 0.004$  models (bottom). Symbols are the same as in Fig. 2.

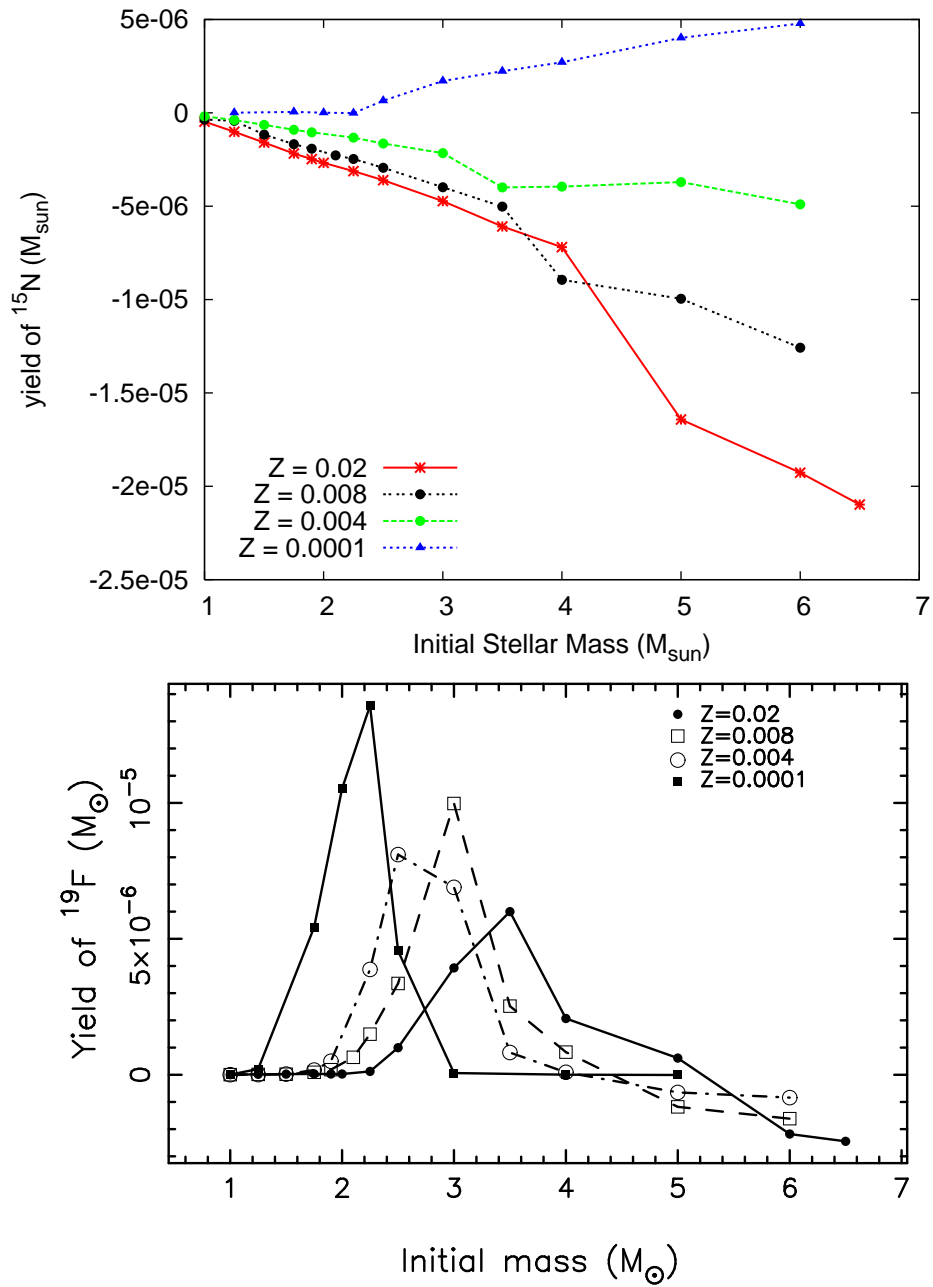


Figure 8: Unweighted yield of  $^{15}\text{N}$  (top panel) and  $^{19}\text{F}$  (lower panel) as a function of the initial mass and metallicity  $Z$ .

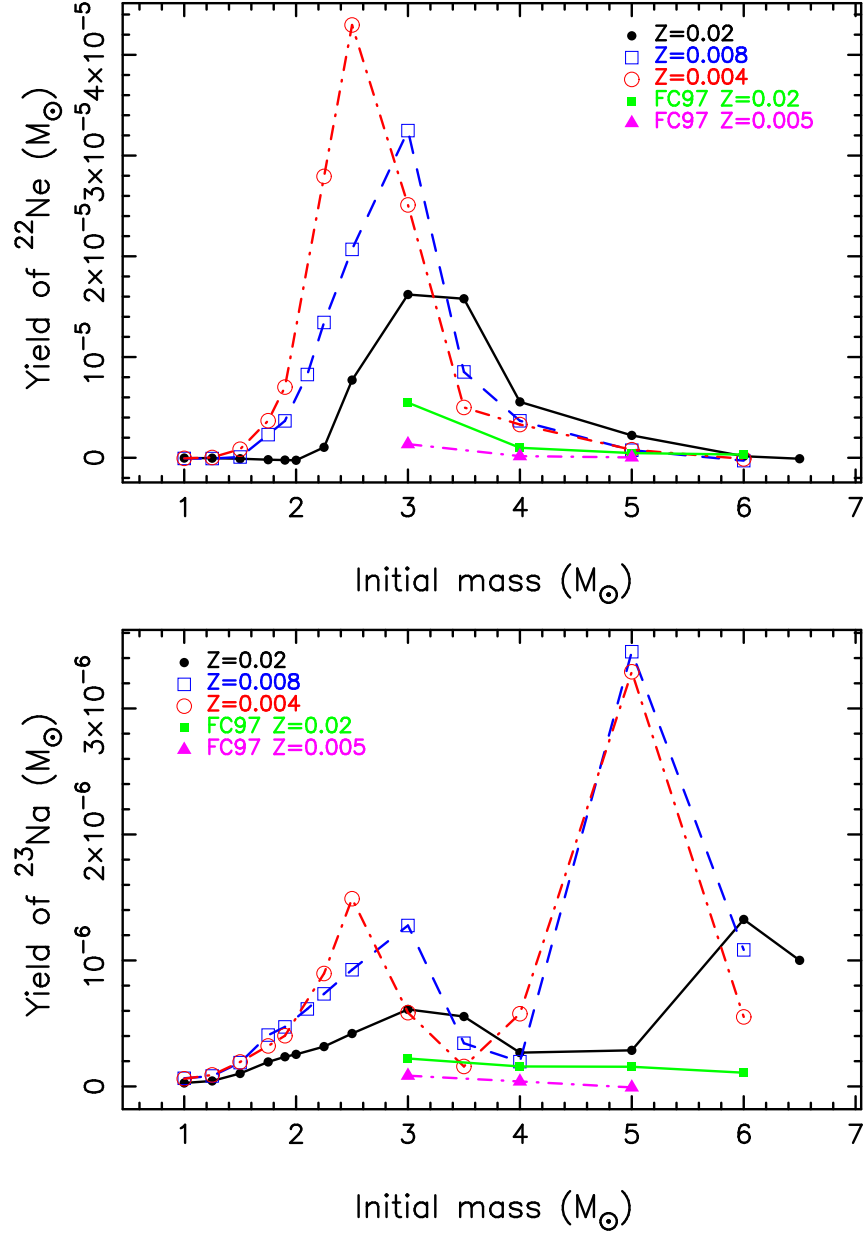


Figure 9: Weighted  $^{22}\text{Ne}$  (top panel) and  $^{23}\text{Na}$  (lower panel) yields and for the  $Z = 0.02$ , the  $Z = 0.008$  and  $Z = 0.004$  models. The yields of Forestini & Charbonnel (1997) are also shown.



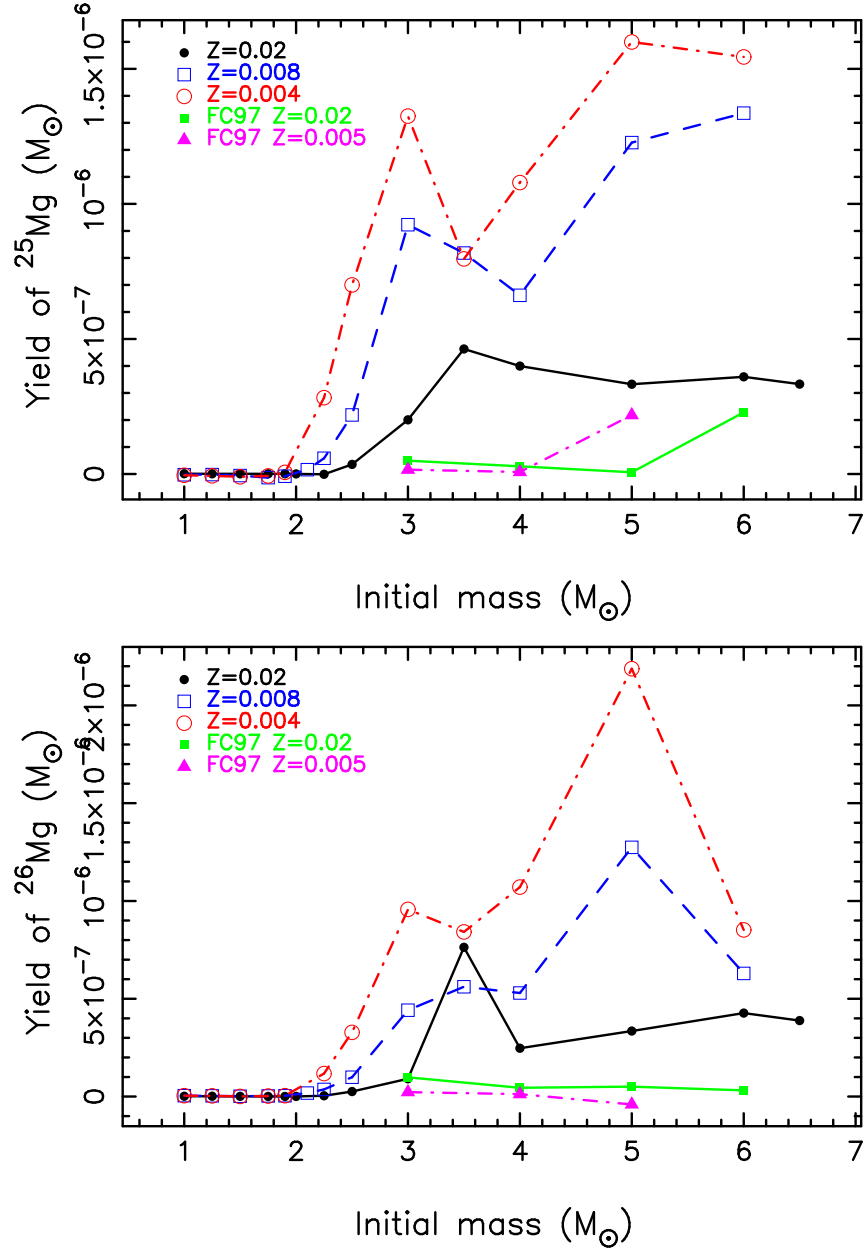


Figure 10: Weighted  $^{25}\text{Mg}$  (top panel) and  $^{26}\text{Mg}$  (lower panel) yields and for the  $Z = 0.02$ , the  $Z = 0.008$  and  $Z = 0.004$  models. The yields of Forestini & Charbonnel (1997) are also shown.

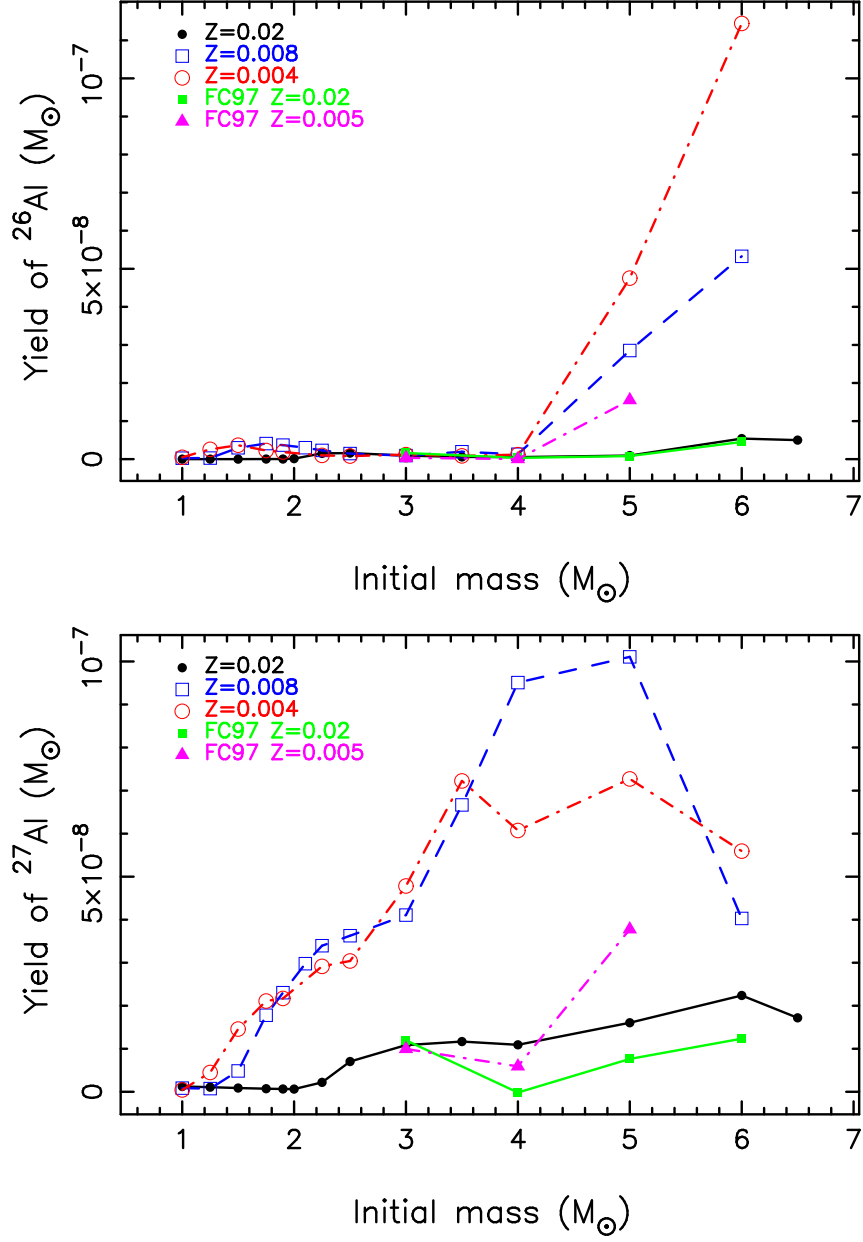


Figure 11: Weighted  $^{26}\text{Al}$  (top panel) and  $^{27}\text{Al}$  (lower panel) yields and for the  $Z = 0.02$ , the  $Z = 0.008$  and  $Z = 0.004$  models. The yields of Forestini & Charbonnel (1997) are also shown.

## 5 Conclusions

We present stellar structure data and yields from detailed AGB models with initial masses between 1 to  $6M_{\odot}$ , and with metallicities in the range from solar to  $1/200^{\text{th}}$  of the solar metallicity. All models were evolved from the zero-age main sequence to near the tip of the AGB track, from there we used a synthetic AGB algorithm to estimate the contribution of any remaining TPs. All results are presented in tabulated form and are available for download. These data are useful for many applications including comparison to other detailed AGB models, for use in galactic chemical evolution studies and for comparison to the composition of AGB stars, planetary nebulae and other post-AGB objects, as well as pre-solar grains. Such a comparison may help shed light on the model uncertainties that affect the yields, such as the mass-loss rate or nuclear reaction rates. Future work will involve running scaled-solar models for the intermediate-metallicities ( $Z = 0.008, 0.004$ ) and adding more nuclei in the post-processing nuclear network to enable us to provide yields for *s*-process elements. Future work should also look at some of the reasons for convergence problems in the stellar models near the tip of the AGB, and include more physics into the calculations such as extra-mixing in low-mass AGB stars.

## Acknowledgments

AIK gratefully acknowledges support from the Australian Research Council's Discovery Projects funding scheme (project number DP0664105). JCL thanks the ARC for support. We also thank the referee, Carlos Abia, for instructive comments that have helped to improve the manuscript.

## References

- Abia, C. & Isern, J. 1997, MNRAS, 289, L11
- Anders, E. & Grevesse, N. 1989, Geochim. Cosmochim. Acta, 53, 197
- Asplund, M., Grevesse, N., & Sauval, A. J. 2005, in ASP Conf. Ser. 336: Cosmic Abundances as Records of Stellar Evolution and Nucleosynthesis, ed. T. G. Barnes, III & F. N. Bash, 25
- Beers, T. C. & Christlieb, N. 2005, ARA&A, 43, 531
- Blöcker, T. 1995, A&A, 297, 727
- Bloecker, T. & Schoenberner, D. 1991, A&A, 244, L43
- Boothroyd, A. I. & Sackmann, I.-J. 1988, ApJ, 328, 653
- Boothroyd, A. I., Sackmann, I.-J., & Ahern, S. C. 1993, ApJ, 416, 762
- Boothroyd, A. I., Sackmann, I.-J., & Wasserburg, G. J. 1995, ApJ, 442, L21
- Busso, M., Gallino, R., & Wasserburg, G. J. 1999, ARA&A, 37, 239
- Campbell, S. W. 2007, PhD thesis, Monash University
- Cannon, R. C. 1993, MNRAS, 263, 817
- Charbonnel, C. 1994, A&A, 282, 811
- Charbonnel, C. & Zahn, J.-P. 2007, A&A, 467, L15
- Dearborn, D. S. P., Lattanzio, J. C., & Eggleton, P. P. 2006, ApJ, 639, 405
- Denissenkov, P. A. & Herwig, F. 2003, ApJ, 590, L99
- Dinerstein, H. L., Richter, M. J., Lacy, J. H., & Sellgren, K. 2003, AJ, 125, 265
- Dopita, M. A., Vassiliadis, E., Wood, P. R., Meatheringham, S. J., Harrington, J. P., Bohlin, R. C., Ford, H. C., Stecher, T. P., & Maran, S. P. 1997, ApJ, 474, 188
- Eggleton, P. P., Dearborn, D. S. P., & Lattanzio, J. C. 2006, Science, 314, 1580
- . 2007, ApJ, submitted
- Fenner, Y., Campbell, S., Karakas, A. I., Lattanzio, J. C., & Gibson, B. K. 2004, MNRAS, 353, 789

- Forestini, M. & Charbonnel, C. 1997, *A&AS*, 123, 241
- Frogel, J. A., Mould, J., & Blanco, V. M. 1990, *ApJ*, 352, 96
- Frost, C. A., Cannon, R. C., Lattanzio, J. C., Wood, P. R., & Forestini, M. 1998, *A&A*, 332, L17
- Frost, C. A. & Lattanzio, J. C. 1996, *ApJ*, 473, 383
- Garcia-Hernandez, D. A., Garcia-Lario, P., Plez, B., D'Antona, F., Manchado, A., & Trigo-Rodriguez, J. M. 2006, *Science*, 314, 1751
- Garcia-Hernandez, D. A., Garcia-Lario, P., Plez, B., Manchado, A., D'Antona, F., Lub, J., & Habing, H. 2007, *A&A*, 462, 711
- Goriely, S. & Mowlavi, N. 2000, *A&A*, 362, 599
- Gratton, R., Sneden, C., & Carretta, E. 2004, *ARA&A*, 42, 385
- Groenewegen, M. A. T. & de Jong, T. 1993, *A&A*, 267, 410
- Guandalini, R., Busso, M., Ciprini, S., Silvestro, G., & Persi, P. 2006, *A&A*, 445, 1069
- Henry, R. B. C. 1989, *MNRAS*, 241, 453
- Herwig, F. 2004a, *ApJ*, 605, 425
- . 2004b, *ApJS*, 155, 651
- . 2005, *ARA&A*, 43, 435
- Izzard, R. G. and Dray, L. M., Karakas, A. I., Lugaro, M., & Tout, C. A. 2006, *A&A*, 460, 565
- Izzard, R. G., Lugaro, M., Karakas, A. I., Iliadis, C., & van Raai, M. 2007, *A&A*, 466, 641
- Izzard, R. G., Tout, C. A., Karakas, A. I., & Pols, O. R. 2004, *MNRAS*, 350, 407
- Jorissen, A., Smith, V. V., & Lambert, D. L. 1992, *A&A*, 261, 164
- Kaler, J. B. 1978, *ApJ*, 225, 527
- Karakas, A. I. 2003, PhD thesis, Monash University
- Karakas, A. I., Fenner, Y., Sills, A., Campbell, S. W., & Lattanzio, J. C. 2006a, *ApJ*, 652, 1240
- Karakas, A. I. & Lattanzio, J. C. 2003, *PASA*, 20, 279
- Karakas, A. I., Lattanzio, J. C., & Pols, O. R. 2002, *PASA*, 19, 515
- Karakas, A. I., Lugaro, M., & Gallino, R. 2007, *ApJ*, 656, L73
- Karakas, A. I., Lugaro, M., Wiescher, M., Goerres, J., & Ugalde, C. 2006b, *ApJ*, 643, 471
- Kroupa, P., Tout, C. A., & Gilmore, G. 1993, *MNRAS*, 262, 545
- Lattanzio, J., Frost, C., Cannon, R., & Wood, P. R. 1996, *Mem. Soc. Astron. Italiana*, 67, 729
- Lattanzio, J. C. 1986, *ApJ*, 311, 708
- . 1992, *PASA*, 10, 120
- Lugaro, M., Karakas, A. I., Nittler, L. R., Alexander, C. M. O., Hoppe, P., Iliadis, C., & Lattanzio, J. C. 2007, *A&A*, 461, 657
- Lugaro, M., Ugalde, C., Karakas, A. I., Görres, J., Wiescher, M., Lattanzio, J. C., & Cannon, R. C. 2004, *ApJ*, 615, 934
- Marigo, P. 2001, *A&A*, 370, 194
- Marigo, P., Bressan, A., & Chiosi, C. 1996, *A&A*, 313, 545
- McSaveney, J. A., Wood, P. R., Scholz, M., Lattanzio, J. C., & Hinkle, K. H. 2007, *MNRAS*, in press

- Mowlavi, N. 1999, *A&A*, 344, 617
- Nollett, K. M., Busso, M., & Wasserburg, G. J. 2003, *ApJ*, 582, 1036
- Paczynski, B. 1975, *ApJ*, 202, 558
- Palacios, A., Charbonnel, C., Talon, S., & Siess, L. 2006, *A&A*, 453, 261
- Plez, B., Smith, V. V., & Lambert, D. L. 1993, *ApJ*, 418, 812
- Reimers, D. 1975, Circumstellar envelopes and mass loss of red giant stars (Problems in stellar atmospheres and envelopes.), 229–256
- Renzini, A. & Voli, M. 1981, *A&A*, 94, 175
- Russell, S. C. & Dopita, M. A. 1992, *ApJ*, 384, 508
- Sharpee, B., Zhang, Y., Williams, R., Pellegrini, E., Cavagnolo, K., Baldwin, J. A., Phillips, M., & Liu, X.-W. 2007, *ApJ*, 659, 1265
- Siess, L. 2006, *A&A*, 448, 717
- Smith, V. V. & Lambert, D. L. 1989, *ApJ*, 345, L75
- . 1990, *ApJ*, 361, L69
- Stancliffe, R. J., Izzard, R. G., & Tout, C. A. 2005, *MNRAS*, 356, L1
- Stancliffe, R. J., Izzard, R. G., Tout, C. A., & Pols, O. R. 2004, *Mem. Soc. Astron. Italiana*, 75, 670
- Stancliffe, R. J. & Jeffery, C. S. 2007, *MNRAS*, 375, 1280
- Stanghellini, L., Guerrero, M. A., Cunha, K., Machado, A., & Villaver, E. 2006, *ApJ*, 651, 898
- Stanghellini, L., Shaw, R. A., Balick, B., & Blades, J. C. 2000, *ApJ*, 534, L167
- Sterling, N. C. & Dinerstein. 2007, *ApJS*, accepted
- Sterling, N. C., Dinerstein, H. L., & Bowers, C. W. 2002, *ApJ*, 578, L55
- Straniero, O., Chieffi, A., Limongi, M., Busso, M., Gallino, R., & Arlandini, C. 1997, *ApJ*, 478, 332
- Thielemann, F.-K., Truran, J. W., & Arnould, M. 1986, in *Advances in Nuclear Astrophysics*, ed. E. Vangioni-Flam, J. Audouze, M. Casse, J.-P. Chieze, & J. Tran Thanh van, 525–540
- van den Hoek, L. B. & Groenewegen, M. A. T. 1997, *A&AS*, 123, 305
- van Winckel, H. 2003, *ARA&A*, 41, 391
- Vassiliadis, E. & Wood, P. R. 1993, *ApJ*, 413, 641
- Ventura, P. & D’Antona, F. 2005a, *A&A*, 431, 279
- . 2005b, *A&A*, 439, 1075
- Ventura, P., D’Antona, F., & Mazzitelli, I. 2002, *A&A*, 393, 215
- Wagenhuber, J. & Groenewegen, M. A. T. 1998, *A&A*, 340, 183
- Wallerstein, G. & Knapp, G. R. 1998, *ARA&A*, 36, 369
- Wood, P. R., Bessell, M. S., & Fox, M. W. 1983, *ApJ*, 272, 99
- Yong, D., Grundahl, F., Lambert, D. L., Nissen, P. E., & Shetrone, M. D. 2003, *A&A*, 402, 985

Table 2: Data for the  $3M_{\odot}$ ,  $Z = 0.02$  model.

Pulse	$M_{\text{core}}$	$M_{\text{csh}}$	$t_{\text{csh}}$	$\Delta M_{\text{dredge}}$	$\lambda$	$\lambda_{\text{dup}}$
1	5.763726E-01	2.237684E-02	3.339341E+02	0.000000E+00	0.000000E+00	0.000000E+00
2	5.782992E-01	2.551377E-02	2.015471E+02	0.000000E+00	0.000000E+00	0.000000E+00
3	5.811490E-01	2.586406E-02	2.061110E+02	0.000000E+00	0.000000E+00	0.000000E+00
4	5.850938E-01	2.622330E-02	1.793678E+02	0.000000E+00	0.000000E+00	0.000000E+00
5	5.898175E-01	2.566504E-02	1.954225E+02	0.000000E+00	0.000000E+00	0.000000E+00
6	5.952812E-01	2.515078E-02	1.755154E+02	0.000000E+00	0.000000E+00	0.000000E+00
7	6.012007E-01	2.422720E-02	2.020128E+02	0.000000E+00	0.000000E+00	0.000000E+00
8	6.074721E-01	2.330387E-02	1.798662E+02	0.000000E+00	0.000000E+00	0.000000E+00
9	6.139326E-01	2.226830E-02	1.702774E+02	0.000000E+00	0.000000E+00	0.000000E+00
10	6.205002E-01	2.124983E-02	1.376081E+02	2.955794E-04	4.524140E-02	1.390973E-02
11	6.269240E-01	2.039099E-02	1.702900E+02	6.338358E-04	9.432908E-02	3.108412E-02
12	6.331832E-01	1.966518E-02	1.570454E+02	1.435995E-03	2.083254E-01	7.302221E-02
13	6.389904E-01	1.907504E-02	1.575242E+02	2.473533E-03	3.414993E-01	1.296738E-01
14	6.442509E-01	1.871735E-02	1.404630E+02	3.429413E-03	4.434169E-01	1.832211E-01
15	6.489711E-01	1.843846E-02	1.480161E+02	4.516482E-03	5.541952E-01	2.449490E-01
16	6.531649E-01	1.828820E-02	1.291233E+02	4.803419E-03	5.514702E-01	2.626514E-01
17	6.571379E-01	1.772785E-02	1.474301E+02	5.583823E-03	6.362296E-01	3.149746E-01
18	6.607848E-01	1.762992E-02	1.466641E+02	6.045818E-03	6.549662E-01	3.429294E-01
19	6.641064E-01	1.734108E-02	1.509221E+02	6.349206E-03	6.777933E-01	3.661368E-01
20	6.672819E-01	1.703131E-02	1.502906E+02	6.745815E-03	7.082441E-01	3.960831E-01
21	6.702475E-01	1.687807E-02	1.387330E+02	7.370591E-03	7.589639E-01	4.366964E-01
22	6.729269E-01	1.684576E-02	1.398080E+02	7.480979E-03	7.443761E-01	4.440867E-01
23	6.753748E-01	1.643026E-02	1.353630E+02	7.710814E-03	7.766045E-01	4.693057E-01
24	6.777956E-01	1.632255E-02	1.362144E+02	7.740200E-03	7.639663E-01	4.742027E-01
25	6.800572E-01	1.598930E-02	1.370616E+02	6.662667E-03	6.661482E-01	4.166952E-01

Table 3: Data for the  $3M_{\odot}$ ,  $Z = 0.02$  model continued.

Pulse	$T_{\text{Hshell}}$	$T_{\text{bce}}$	$T_{\text{Hshell}}$	interpulse	$M_{\text{tot}}$	MaxL	MaxLHe
1	1.840110E+08	2.505874E+06	4.832516E+07	0.000000E+00	2.989960E+00	3.297096E+03	2.896448E+04
2	1.969207E+08	2.684860E+06	5.026387E+07	5.221891E+04	2.989959E+00	3.937624E+03	1.183492E+05
3	2.086133E+08	2.863514E+06	5.204397E+07	6.784875E+04	2.989958E+00	4.585147E+03	2.987256E+05
4	2.195342E+08	3.031484E+06	5.371028E+07	8.031166E+04	2.989955E+00	5.245723E+03	7.595382E+05
5	2.269594E+08	3.190444E+06	5.494672E+07	8.659560E+04	2.989951E+00	5.779177E+03	1.319066E+06
6	2.342317E+08	3.365202E+06	5.611659E+07	8.875659E+04	2.989945E+00	6.321060E+03	2.281208E+06
7	2.394346E+08	3.526668E+06	5.707119E+07	8.778255E+04	2.989937E+00	6.797777E+03	3.222215E+06
8	2.440928E+08	3.692101E+06	5.796298E+07	8.513058E+04	2.989924E+00	7.263765E+03	4.398030E+06
9	2.478168E+08	3.866263E+06	5.875260E+07	8.134384E+04	2.989906E+00	7.706778E+03	5.538496E+06
10	2.513340E+08	4.048897E+06	5.950483E+07	7.718683E+04	2.989879E+00	8.141840E+03	6.776800E+06
11	2.551253E+08	4.215980E+06	6.026202E+07	7.320287E+04	2.989840E+00	8.584714E+03	8.464204E+06
12	2.589790E+08	4.410556E+06	6.096342E+07	6.977448E+04	2.989780E+00	9.015570E+03	1.072477E+07
13	2.630434E+08	4.610824E+06	6.166960E+07	6.747551E+04	2.989682E+00	9.461654E+03	1.447887E+07
14	2.682954E+08	4.819258E+06	6.234783E+07	6.636544E+04	2.989504E+00	9.909229E+03	1.847517E+07
15	2.715982E+08	5.026276E+06	6.293235E+07	6.538550E+04	2.989177E+00	1.032697E+04	3.002030E+07
16	2.781746E+08	5.236472E+06	6.348534E+07	6.524187E+04	2.988530E+00	1.073885E+04	4.387040E+07
17	2.808189E+08	5.397694E+06	6.389052E+07	6.336352E+04	2.987350E+00	1.108444E+04	4.838104E+07
18	2.832818E+08	5.603128E+06	6.432855E+07	6.284853E+04	2.985032E+00	1.144775E+04	5.528658E+07
19	2.867869E+08	5.794352E+06	6.465809E+07	6.148713E+04	2.980963E+00	1.176355E+04	8.176797E+07
20	2.898100E+08	6.002216E+06	6.496616E+07	6.025162E+04	2.973891E+00	1.207047E+04	9.513553E+07
21	2.926001E+08	6.200394E+06	6.525625E+07	5.917455E+04	2.962824E+00	1.236732E+04	1.163203E+08
22	2.953747E+08	6.541253E+06	6.554327E+07	5.878434E+04	2.951519E+00	1.266948E+04	1.445130E+08
23	2.972316E+08	6.751874E+06	6.573163E+07	5.686887E+04	2.936666E+00	1.291685E+04	1.500224E+08
24	2.999315E+08	6.557310E+06	6.592716E+07	5.622341E+04	2.845449E+00	1.314644E+04	1.755376E+08
25	3.021500E+08	6.128534E+06	6.598145E+07	5.471787E+04	2.211516E+00	1.323496E+04	1.658657E+08

Table 4: Data used to estimate the number of remaining TPs. We include the final total and core mass after the final TP, as determined by the synthetic AGB program, the  $\lambda$  used for the final TDU episodes, the total number of TPs (including the synthetic TPs) and the number of synthetic TPs. The VW93 indicates the  $5M_{\odot}$ ,  $Z = 0.02$  model that was computed with Vassiliadis & Wood (1993) mass loss on the AGB whereas the R75 indicates data for the model computed with Reimer’s mass loss with  $\eta = 3.5$ .

<i>Z=0.02</i>					
$M_0$	$M_f$	$M_{c,f}$	$\lambda_f$	No. TPs	Syn. TPs
2.5	1.1388	0.6630	0.4584	26	1
3.0	1.3580	0.6819	0.6661	26	1
3.5	1.2675	0.7181	0.8583	22	1
4.0	1.1151	0.7916	0.9306	19	2
5.0 (VW93)	1.2545	0.8757	0.9098	27	4
5.0 (R75)	1.0458	0.8736	0.9516	42	5
6.0	1.1984	0.9294	0.9471	43	5
6.5	0.9918	0.9629	0.8539	46	7
<i>Z=0.008</i>					
2.5	0.9978	0.6626	0.7760	28	1
3.0	1.0077	0.6934	0.8612	29	1
3.5	1.4192	0.7662	0.9530	21	1
4.0	0.9716	0.8367	0.9730	24	2
5.0	1.1631	0.8860	0.9540	61	4
6.0	1.1408	0.9480	0.9195	73	5
<i>Z=0.004</i>					
2.5	1.3578	0.6707	0.8165	29	1
3.5	1.1274	0.8138	0.9720	24	1
4.0	1.0533	0.8524	0.9460	32	1
5.0	1.0138	0.9055	0.9715	84	3
6.0	1.1859	0.9792	0.9515	106	5
<i>Z=0.0001</i>					
2.5	1.1489	0.7325	0.8207	31	1
3.0	1.2758	0.8159	0.9691	40	1
3.5	1.2627	0.8474	0.9505	59	1
4.0	1.1767	0.8694	0.9188	76	1
5.0 (VW93)	1.0374	0.9340	0.9297	138	2
5.0 (R75)	1.2558	0.9244	0.9312	69	1



Table 5: Stellar yields for  $3M_{\odot}$ ,  $Z = 0.02$  model.

Isotope $i$	$A$	yield	mass( $i$ ) <sub>lost</sub>	mass( $i$ ) <sub>0</sub>	$\langle X(i) \rangle$	$X0(i)$	$f$
$g^a$	1	1.0600706E-07	1.2625863E-05	1.2519856E-05	5.4468778E-06	5.4014972E-06	3.6334887E-03
p	1	-8.0847383E-02	1.5124202	1.5932676	6.5246773E-01	6.8739051E-01	-2.2644492E-02
$^3\text{He}$	3	2.2212508E-04	2.2214468E-04	1.9598588E-08	9.5834628E-05	8.4555056E-09	4.0543828
$^4\text{He}$	4	6.1267972E-02	7.4012238E-01	6.7885441E-01	3.1929350E-01	2.9288119E-01	3.7498605E-02
$^7\text{Li}$	7	-1.8814418E-08	6.0166285E-09	2.4831047E-08	2.5956119E-09	1.0712970E-08	-6.1567014E-01
$^{12}\text{C}$	12	1.4943778E-02	2.2845197E-02	7.9014199E-03	9.8555638E-03	3.4089447E-03	4.6106154E-01
$^{13}\text{C}$	13	1.1727007E-04	2.1251373E-04	9.5243653E-05	9.1679773E-05	4.1091393E-05	3.4852266E-01
$^{14}\text{N}$	14	3.3946566E-03	5.8388105E-03	2.4441539E-03	2.5189000E-03	1.0544922E-03	3.7816754E-01
$^{15}\text{N}$	15	-4.7271697E-06	4.8713855E-06	9.5985552E-06	2.1015467E-06	4.1411477E-06	-2.9458165E-01
$^{16}\text{O}$	16	-1.2392532E-03	2.1018269E-02	2.2257522E-02	9.0674153E-03	9.6026622E-03	-2.4908133E-02
$^{17}\text{O}$	17	5.1704166E-05	6.0690640E-05	8.9864743E-06	2.6182328E-05	3.8770745E-06	8.2950413E-01
$^{18}\text{O}$	18	-1.3407498E-05	3.6671925E-05	5.0079423E-05	1.5820502E-05	2.1605989E-05	-1.3535389E-01
$^{19}\text{F}$	19	3.8715425E-06	4.9463952E-06	1.0748529E-06	2.1339065E-06	4.6372855E-07	6.6291153E-01
$^{20}\text{Ne}$	20	-1.1501834E-06	4.1906834E-03	4.1918335E-03	1.8078875E-03	1.8085014E-03	-1.4747151E-04
$^{21}\text{Ne}$	21	4.0954365E-07	1.1120977E-05	1.0711433E-05	4.7976600E-06	4.6212808E-06	1.6267121E-02
$^{22}\text{Ne}$	22	1.9907814E-03	2.3274263E-03	3.3664503E-04	1.0040666E-03	1.4524026E-04	8.3967549E-01
$^{23}\text{Na}$	23	7.5442040E-05	1.6396206E-04	8.8520021E-05	7.0734277E-05	3.8190585E-05	2.6767361E-01
$^{24}\text{Mg}$	24	-8.9756213E-07	1.3679401E-03	1.3688377E-03	5.9013808E-04	5.9056369E-04	-3.1310008E-04
$^{25}\text{Mg}$	25	2.4309760E-05	2.0399288E-04	1.7968312E-04	8.8003828E-05	7.7521494E-05	5.5079415E-02
$^{26}\text{Mg}$	26	1.1070690E-05	2.1723099E-04	2.0616030E-04	9.3714836E-05	8.8944660E-05	2.2688469E-02
$^{26}\text{Al}$	26	1.1710374E-07	1.1710374E-07	0.0000000E+00	5.0519297E-08	0.0000000E+00	0.0000000E+00
$^{27}\text{Al}$	27	1.2958917E-06	1.5529012E-04	1.5399423E-04	6.6993147E-05	6.6438413E-05	3.6111036E-03
$^{28}\text{Si}$	28	-1.6319100E-06	1.7316726E-03	1.7333045E-03	7.4705458E-04	7.4780727E-04	-4.3735650E-04
$^{29}\text{Si}$	29	1.5787009E-06	9.2347655E-05	9.0768954E-05	3.9839368E-05	3.9160856E-05	7.4602445E-03
$^{30}\text{Si}$	30	2.4255860E-07	6.2702733E-05	6.2460174E-05	2.7050359E-05	2.6947471E-05	1.6549942E-03
$^{31}\text{P}$	31	2.0692660E-06	2.3703114E-05	2.1633849E-05	1.0225674E-05	9.3335875E-06	3.9643381E-02
$^{32}\text{S}$	32	-2.1749875E-06	1.0513477E-03	1.0535227E-03	4.5355811E-04	4.5452599E-04	-9.2578813E-04
$^{33}\text{S}$	33	4.0168288E-07	8.9708283E-06	8.5691454E-06	3.8700723E-06	3.6970248E-06	1.9866738E-02
$^{34}\text{S}^b$	34	-1.7065395E-07	4.9333787E-05	4.9504441E-05	2.1282909E-05	2.1357921E-05	-1.5279896E-03
$^{56}\text{Fe}$	56	-2.1018088E-05	3.0820514E-03	3.1030695E-03	1.3296166E-03	1.3387711E-03	-2.9798900E-03
$^{57}\text{Fe}$	57	1.3097335E-05	8.8821595E-05	7.5724260E-05	3.8318201E-05	3.2670057E-05	6.79255233E-02
$^{58}\text{Fe}$	58	7.2211260E-06	1.7037621E-05	9.8164946E-06	7.3501383E-06	4.2351739E-06	2.3942426E-01
$^{60}\text{Fe}$	60	3.9827793E-08	3.9827793E-08	0.0000000E+00	1.7181964E-08	0.0000000E+00	0.0000000E+00
$^{59}\text{Co}$	59	1.4924935E-06	1.0411269E-05	8.9187752E-06	4.4914877E-06	3.8478670E-06	6.7170151E-02
$^{58}\text{Ni}$	58	-2.2356980E-06	1.2900950E-04	1.3124519E-04	5.5655517E-05	5.6623696E-05	-7.4899960E-03
$^{60}\text{Ni}$	60	7.0899841E-07	5.2735955E-05	5.2026957E-05	2.2750626E-05	2.2446222E-05	5.8501000E-03
$^{61}\text{Ni}$	61	8.3594359E-06	1.0636427E-05	2.2769907E-06	4.5886222E-06	9.8237228E-07	6.6940618E-01
$^{62}\text{Ni}$	62	-7.3240267E-06	5.0168190E-08	7.3741949E-06	2.1642876E-08	3.1814818E-06	-2.1673145E+00

<sup>a</sup>  $g$  represents the abundance of species from  $^{64}\text{Ni}$  to Bi; an increase in  $g$  indicates that neutron-captures have occurred beyond the end of the network.<sup>b</sup>  $^{34}\text{S}$  includes the abundance of species between  $^{34}\text{S}$  and Mn.

Table 6: PN yields  $3M_{\odot}$ ,  $Z = 0.02$  model. The first entry is the total mass ejected during the final two TPs,  $1.502M_{\odot}$  in this case.

Isotope $i$	$A$	yield	mass( $i$ ) <sub>lost</sub>	$X0(i)$	$\langle X(i) \rangle$	$N(i)/N(H)$
g	1	9.4299139E-08	8.2076585E-06	5.4014972E-06	5.4642769E-06	8.3678888E-06
p	1	-5.1648498E-02	9.8085165E-01	6.8739051E-01	6.5300536E-01	1.0000000E+00
<sup>3</sup> He	3	1.4400885E-04	1.4402156E-04	8.4555056E-09	9.5882846E-05	4.8944388E-05
<sup>4</sup> He	4	3.9245605E-02	4.7917002E-01	2.9288119E-01	3.1900910E-01	1.2213111E-01
<sup>7</sup> Li	7	-1.2191149E-08	3.9003480E-09	1.0712970E-08	2.5966702E-09	5.6807015E-10
<sup>12</sup> C	12	9.4264597E-03	1.4546891E-02	3.4089447E-03	9.6846428E-03	1.2359064E-03
<sup>13</sup> C	13	7.6098098E-05	1.3781973E-04	4.1091393E-05	9.1753966E-05	1.0808482E-05
<sup>14</sup> N	14	2.2036042E-03	3.7875122E-03	1.0544922E-03	2.5215494E-03	2.7581805E-04
<sup>15</sup> N	15	-3.0603858E-06	3.1598568E-06	4.1411477E-06	2.1036856E-06	2.1476960E-07
<sup>16</sup> O	16	-7.9538208E-04	1.3628369E-02	9.6026622E-03	9.0731336E-03	8.6840155E-04
<sup>17</sup> O	17	3.3530909E-05	3.9354498E-05	3.8770745E-06	2.6200392E-05	2.3601635E-06
<sup>18</sup> O	18	-8.6711771E-06	2.3782261E-05	2.1605989E-05	1.5833122E-05	1.3470301E-06
<sup>19</sup> F	19	2.4399674E-06	3.1365144E-06	4.6372855E-07	2.0881453E-06	1.6830241E-07
<sup>20</sup> Ne	20	-8.7078661E-07	2.7156025E-03	1.8085014E-03	1.8079218E-03	1.3843084E-04
<sup>21</sup> Ne	21	2.5139525E-07	7.1928253E-06	4.6212808E-06	4.7886483E-06	3.4920211E-07
<sup>22</sup> Ne	22	1.2537986E-03	1.4719579E-03	1.4524026E-04	9.7996101E-04	6.8213347E-05
<sup>23</sup> Na	23	4.7911446E-05	1.0527590E-04	3.8190585E-05	7.0087794E-05	4.6665705E-06
<sup>24</sup> Mg	24	-5.7858415E-07	8.8648207E-04	5.9056369E-04	5.9017848E-04	3.7657839E-05
<sup>25</sup> Mg	25	1.4788740E-05	1.3123048E-04	7.7521494E-05	8.7367145E-05	5.3516951E-06
<sup>26</sup> Mg	26	6.7903602E-06	1.4039036E-04	8.8944660E-05	9.3465365E-05	5.5050414E-06
<sup>26</sup> Al	26	7.8603932E-08	7.8603932E-08	0.0000000E+00	5.2330840E-08	3.0822480E-09
<sup>27</sup> Al	27	8.2996121E-07	1.0062428E-04	6.6438413E-05	6.6990964E-05	3.7995808E-06
<sup>28</sup> Si	28	-1.0048971E-06	1.1222448E-03	7.4780727E-04	7.4713834E-04	4.0862618E-05
<sup>29</sup> Si	29	9.7531665E-07	5.9797174E-05	3.9160856E-05	3.9810177E-05	2.1022256E-06
<sup>30</sup> Si	30	1.4533725E-07	4.0621992E-05	2.6947471E-05	2.7044231E-05	1.3805007E-06
<sup>31</sup> P	31	1.2756063E-06	1.5295192E-05	9.3335875E-06	1.0182827E-05	5.0302543E-07
<sup>32</sup> S	32	-1.3433164E-06	6.8138086E-04	4.5452599E-04	4.5363166E-04	2.1708838E-05
<sup>33</sup> S	33	2.5333611E-07	5.8064797E-06	3.6970248E-06	3.8656840E-06	1.7938892E-07
<sup>34</sup> S	34	-1.0619988E-07	3.1974625E-05	2.1357921E-05	2.1287216E-05	9.5878931E-07
<sup>56</sup> Fe	56	-1.3052253E-05	1.9978590E-03	1.3387711E-03	1.3300815E-03	3.6372523E-05
<sup>57</sup> Fe	57	8.2095721E-06	5.7281879E-05	3.2670057E-05	3.8135608E-05	1.0245640E-06
<sup>58</sup> Fe	58	4.4331669E-06	1.0794642E-05	4.2351739E-06	7.1865697E-06	1.8974787E-07
<sup>60</sup> Fe	60	2.0917762E-08	2.0917762E-08	0.0000000E+00	1.3926072E-08	3.5543535E-10
<sup>59</sup> Co	59	9.3833069E-07	6.7180481E-06	3.8478670E-06	4.4725639E-06	1.1608812E-07
<sup>58</sup> Ni	58	-1.3969257E-06	8.3655119E-05	5.6623696E-05	5.5693683E-05	1.4704869E-06
<sup>60</sup> Ni	60	4.3515684E-07	3.4150675E-05	2.2446222E-05	2.2735929E-05	5.8028951E-07
<sup>61</sup> Ni	61	5.3855811E-06	6.8611607E-06	9.8237228E-07	4.5678416E-06	1.1467385E-07
<sup>62</sup> Ni	62	-4.7543513E-06	2.4417719E-08	3.1814818E-06	1.6256180E-08	4.0152268E-10

